

Summer 2018

# Characterization of Eight Potentially Hazardous Near Earth Asteroids: Rotation Period Analysis and Structure Modeling Via Light Curve Inversion Techniques

Stacy Jo Hicks

Western Kentucky University, [stacy.hancock053@topper.wku.edu](mailto:stacy.hancock053@topper.wku.edu)

Follow this and additional works at: <https://digitalcommons.wku.edu/theses>



Part of the [Physics Commons](#), and the [The Sun and the Solar System Commons](#)

---

## Recommended Citation

Hicks, Stacy Jo, "Characterization of Eight Potentially Hazardous Near Earth Asteroids: Rotation Period Analysis and Structure Modeling Via Light Curve Inversion Techniques" (2018). *Masters Theses & Specialist Projects*. Paper 3060.  
<https://digitalcommons.wku.edu/theses/3060>

This Thesis is brought to you for free and open access by TopSCHOLAR®. It has been accepted for inclusion in Masters Theses & Specialist Projects by an authorized administrator of TopSCHOLAR®. For more information, please contact [topscholar@wku.edu](mailto:topscholar@wku.edu).

CHARACTERIZATION OF EIGHT POTENTIALLY HAZARDOUS NEAR EARTH  
ASTEROIDS: ROTATION PERIOD ANALYSIS AND STRUCTURE MODELING  
VIA LIGHT CURVE INVERSION TECHNIQUES

A Thesis  
Presented to  
The Faculty of the Department of Physics and Astronomy  
Western Kentucky University  
Bowling Green, KY

In Partial Fulfillment  
Of the Requirement for the Degree  
Master of Science


By  
Stacy Hicks

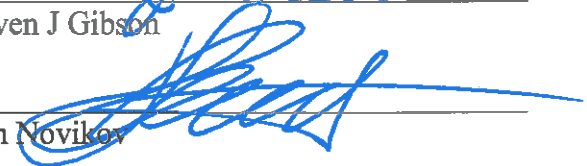
August 2018

CHARACTERIZATION OF EIGHT POTENTIALLY HAZARDOUS NEAR-EARTH  
ASTEROIDS: ROTATION PERIOD ANALYSIS AND STRUCTURE MODELING VIA  
LIGHT CURVE INVERSION TECHNIQUES

Date Recommended 19 July 2018

  
\_\_\_\_\_  
Michael T Carini, Director of Thesis

  
\_\_\_\_\_  
Steven J Gibson

  
\_\_\_\_\_  
Ivan Novikov

 7/19/18  
\_\_\_\_\_  
Dean, Graduate Studies and Research      Date

## ACKNOWLEDGEMENTS

I would like to thank my mentor, Dr. Michael Carini, for his guidance and support throughout my undergraduate and graduate career at Western Kentucky University. I would also like to thank the members of my committee, Dr. Ivan Novikov, Dr. Steven Gibson, and Dr. Michael Carini, for their advice and guidance. A special thank you Ms. Sharon Windham for her administrative support and “therapy” sessions; and Dr. Douglas Harper for help with programming and for allowing me to sit in on his classes to acquire the knowledge I needed to complete this thesis.

A special thank you to Carl Hergenrother and Delores Hill, NASA OSIRIS-REx Target Asteroids Leads, for providing me the opportunity to be part of the OSIRIS-REx mission and allowing access to Target Asteroids data, and for their guidance along the way. Thank you to Dr. Patrick Miller of the International Astronomical Search Collaboration. I would also like to thank NASA/Kentucky Graduate Fellowship for funding this project.

A special thank you to my friends and family for their love and support without which I could not have made it through this journey. I would also like to thank the entire WKU Department of Physics and Astronomy for making WKU feel like home.

## CONTENTS

Chapter 1: Introduction.....	1
Background.....	1
Detection & Classification of NEAs and PHAs.....	5
Scope of Project.....	8
Asteroid Characteristics & Characterization.....	10
Rotation Period & Structural Classification.....	13
Impact Mitigation & Risk Classification.....	14
Targets Background.....	17
Phaethon.....	17
Icarus.....	18
Hathor.....	19
Bede.....	20
2004 JN 13.....	20
2002 FG 7.....	21
2004 QQ.....	21
2004 BL 86.....	21
Chapter 2: Data & Methods.....	23

RCT Observations.....	23
Target Asteroids Observations.....	23
ALCDEF Photometry Database.....	23
Data Processing.....	24
Chaper 3: Analysis Techniques.....	27
Lomb-Scargle Time Series Analysis.....	27
Light Curve Inversion Techniques.....	29
Convex Inversion.....	29
Determination of Pole & Rotation Period.....	32
Treatment of Data.....	32
Chaper 4: Period Determination & Structure Modeling.....	33
Phaethon.....	34
Icarus.....	36
Hathor.....	37
Bede.....	39
2004 JN 13.....	42
2002 FG 7.....	44
2004 QQ.....	45

2004 BL 86.....	46
Structure Modeling.....	48
2002 FG7.....	49
2004 JN13.....	50
Icarus.....	51
Chapter 5: Conclusions.....	53
Future Work.....	56
References.....	57
Appendix: Abbreviations & Symbols.....	65

## List of Tables

Table 1: Number of known asteroids per orbit classification.....	11
Table 2: Summary of observations via source.....	24
Table 3: Summary of data per target for structure modeling.....	31
Table 4: Summary of data used in light curve inversion modeling.....	49
Table 5: Rotation period results summary .....	54
Table 6: Inversion structure modeling results summary.....	54



CHARACTERIZATION OF EIGHT POTENTIALLY HAZARDOUS NEAR EARTH  
ASTEROIDS: ROTATION PERIOD ANALYSIS AND STRUCTURE MODELING  
VIA LIGHT CURVE INVERSION TECHNIQUES

Stacy Hicks

August 2018

66 Pages

Directed by: Michael Carini, Steven Gibson, and Ivan Novikov

Department of Physics and Astronomy

Western Kentucky University

The term “homeland security”, seems to have become synonymous with terrorism in the minds of the general public. However, there are other threats to the security of the United States homeland that can be just as, if not more, devastating than terrorism. Included among these other threats is the potential of an asteroid collision with Earth. Historically, asteroid impact events have been responsible for the devastation of our planet and many of the mass extinction events encountered throughout the geologic record. Knowledge of physical parameters such as structure and rotational dynamics of the asteroid are critical parameters in developing interception and deflection techniques, as well as assessing the risk associated with these bodies and mitigation planning in the event of impact. This thesis encompasses the study of eight potentially hazardous asteroids identified in conjunction with NASA’s OSIRIS REX Mission and observed via the Target Asteroid Project, along with observations from the Robotically Controlled Telescope, and the Asteroid Light Curve Database of Photometry. Photometric data was extracted from all observations. Rotation periods of each target were confirmed using Lomb-Scargle time series analysis, with possible secondary periods indicated in the cases of Hathor (2.2169 hours), Bede (161.1501 hours), and Phaethon (4.5563 hours). Shape models for 2002 FG7, 2004 JN13, and Icarus were produced using light curve inversion techniques These are believed to be the first such models for these asteroids.

# Chapter 1

## Introduction

Threats to homeland security come in many forms. Most people, when they hear the words “homeland security”, immediately think of terrorism and the many threats it poses to homeland security: radiological threats, chemical threats, biological threats, and terrorist attacks such as those we have seen in the past (the coordinated attacks using airplanes on September 11, 2001) or the more recent attacks overseas such as the shootings in France. However, there are other threats to the security of the United States homeland that can be just as, if not more, devastating than terrorism. Included among these are threats related to devastating weather events and the potential of an asteroid collision with Earth.

### *Background*

We only have to look at the landscape of our planet or that of the moon to see the evidence that impacts from bodies from space is part of our planet’s history and likely its future. There are 170 established impact craters on earth’s exposed land surface (Space Studies Board of the National Research Council, 2008). It is estimated that impacts from small asteroids occur at a rate of 5-10 events per year (“Interactive Map of Meteor Strikes”, 2017). Most of these go unnoticed as small objects disintegrate before reaching the ground. If the object does survive the journey through earth’s atmosphere, it is statistically more likely to land in the ocean than on land. From meteor observations, small dust and stony fragments strike our atmosphere resulting in a momentary burst of light at a rate of about 1,000 visible meteors per second across the planet. Larger fragments entering earth’s atmosphere are observed as extremely brilliant meteor-like flashes. Fireballs are meteors

of magnitude  $-4$  or brighter on the standard astronomical magnitude scale. Bolide events are observed as a brilliant flash of light of magnitude  $-14$  or brighter and super-bolide events are of  $-17$  or brighter magnitude.

Meteoroids larger than 1 m are capable of penetrating the earth's atmosphere deep enough to result in an airburst, an event in which the entering objects explodes releasing large amounts of energy comparable to a TNT explosion (Barentsen, 2013). The energy released in an explosion of one ton of TNT is approximately  $4.2 \times 10^{15}$  joules. The standard unit of energy in describing impact event is given in terms of kilotons of TNT. There is an inverse relationship between object size and impact frequency. From analysis of lunar craters, impact frequency decreases proportionally to the cube of the diameter of the asteroid (Marcus et. al. 2010). A study by Brown et. al. 2002, using data from US Defense and Energy Departments' classified data from surveillance satellites along with data from ground based observations analyzed 300 bolide events from 1994 to 2002, comparing event frequency with energy released and diameter of object. The results of that study are shown in Figure 2.

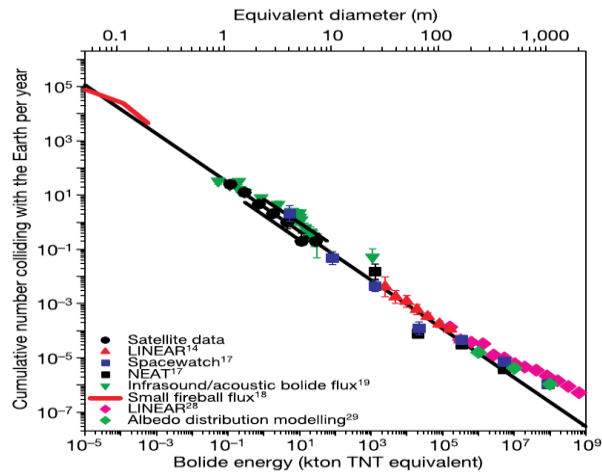


Figure 1: Frequency of impacts as a function of energy (Brown et. al., 2002)

It is estimated that 4 meter stony asteroids hit earth approximately every 1.3 years with kinetic energy of 3 kiloton TNT upon atmospheric entry and 0.75 kiloton TNT upon airburst. Asteroids in the 7 meter diameter range hit earth every 4.6 years with kinetic energy equivalent to 15 kiloton TNT, comparable to the Hiroshima bomb. Asteroids in the 20 meter diameter range, capable of substantial regional damage, strike earth approximately every 60 years. Larger asteroids capable of global impact strike earth less frequently; 1 km objects impact earth about every 440,000 years, and 5 km asteroids strike approximately every 20 million years. (Marcus et. al. 2010)

Impact events involving asteroids 3 km or greater in diameter cross the Threshold of Global Catastrophe, releasing energy equivalent to 10 million megatons of TNT. The Threshold of Global Catastrophe refers to an event which could potentially devastate human civilization and all life on a global scale, resulting in mass extinction of many species. Impact events of this magnitude can result in a chain reaction, triggering massive earthquakes and volcanic activity, adding to and prolonging the devastation to life on earth. Such an event occurred 65 million years ago, when a 12 km asteroid struck earth, impacting what is now known as the Yucatan Peninsula, resulting in the extinction of 70% of all living species, including dinosaurs. The impact left a crater 180 km in diameter, called the Chixulub Crater (Space Studies Board of the National Research Council, 2008).

Fortunately, modern impact events have been less devastating. Probably the most famous modern impact is the 1908 Tunguska event, in which a 45 meter asteroid exploded in an airburst releasing the energy equivalent of many megatons TNT, leveling 2000 square km of Siberian forest (Space Studies Board of the National Research Council, 2008). Due to the remote location, there were no confirmable human casualties from the event,

although people were reportedly knocked to the ground from the shockwave some 60 miles away.

The most recent major impact event occurred February 15, 2013, when a 20 meter asteroid exploded in an airburst 29.7 km above the earth's surface over Chelyabinsk, Russia. The explosion released the equivalent of 500 kilotons TNT of energy; 20-30 times more powerful than the Hiroshima bomb. The event injured 1500 people and caused \$33 million worth of property damage. Alarmingly, the asteroid was undetected until it entered the atmosphere. Coincidentally, the close approach of another asteroid, 2012 DA14, was being monitored that same day. Figure 2, developed by the B612 Foundation, shows the location and approximate impact energy of asteroid (or comet) impacts from 2000 to 2013. This data was taken from low-frequency microphones run by the Comprehensive Nuclear Test Ban Treaty Organization designed to detect nuclear explosions (B612 Foundation, 2017).



Figure 2: Global map of asteroid impacts from 2000-2013. (Courtesy of B612 Foundation).

Asteroids are leftover remnants from the formation of the solar system 4.6 billion years ago. The majority of asteroids in our solar system are found orbiting the sun in the asteroid belt, a region which lies between the orbits of Mars and Jupiter. The gravitational force from Jupiter prevented planets from forming in this regions and subsequent collisions and fragmenting of rocky planetary material formed the asteroid belt. Officially, the largest known asteroid in the asteroid belt is Vesta with a diameter of 530 km. Typically bodies in the asteroid belt have a separation of 1-3 million km, however, their orbits can cross resulting in collisions which can cause fragmenting and sometimes the entrapment of a small asteroid by a larger asteroid which then becomes a binary system. There are 150 asteroids known to have “moons” (smaller asteroids). The asteroid belt is estimated to contain 1.1 to 1.9 million asteroids larger than 1 km and millions of smaller bodies. (“Asteroids in Depth”, 2017)

Asteroids are not only found in the asteroid belt; it is estimated that Trojan asteroids are just as numerous as main belt asteroids. Trojan asteroids share an orbit with a planet, residing in the planet’s L4 and L5 Lagrange points, where the gravitational pull from the sun and planet are equal and the asteroid is held in this equilibrium position. Trojan asteroids have been found orbiting with Mars, Neptune, and Earth. (NEO Basics, 2017)

### ***Detection & Classification of NEAs and PHAs***

An asteroid is classified as a Near Earth Asteroid (NEA) or Near Earth Object (NEO), (includes asteroids and comets greater than 140 meter in size) if the object’s orbital trajectory comes within 1.3 AU, which corresponds to a Minimum Orbit Intersection Distance (MOID) of 0.3 AU with respect to earth’s orbit. As of 2016, more than 15,000 NEAs have been discovered, a 50% increase since 2013. Of these, 95% were discovered

from NASA funded surveys. Potentially Hazardous Asteroids (PHAs) are classified as bodies with MOID 0.05 AU and having absolute magnitude (H)<sup>1</sup> less than 22, which implies a diameter of larger than 140 meters. (Planetary Defense Frequently Asked Questions, 2017). The Near Earth Object Wide-Field Survey Explorer (NEOWISE) program estimates that there are  $4700 \pm 1500$  PHAs with diameters greater than 100 meters, only 20-30% of which have been discovered. On average there are several close “flybys” from PHAs each month.

All asteroid discoveries are reported to the Minor Planet Center (MPC), operated by the International Astronomical Union (IAU) and funded by NASA. MPC keeps an up to date, publicly assessable catalogue of all NEOs, as well as a database of available light curve data for asteroids, orbital elements, and an ephemeris generator. MPC also coordinates confirmation of asteroid discoveries by follow up observations. Once confirmed, MPC assigns a provisional designation to the asteroid, typically consisting of the year of discovery followed by two letters, the first of which indicates the half-month in which the discovery was made, and the second indicates the order of discovery within that half-month.

The discovery of known asteroids can be attributed to contributions from both amateur observers and professional agencies. Several large scale operations have resulted in the discovery of thousands of asteroids. Among these projects is the Near Earth Object Wide-Field Survey Explorer (NEOWISE) survey, managed by NASA’s Jet Propulsion

---

<sup>1</sup> In this context, absolute magnitude is the visual magnitude an observer would record if the asteroid were placed 1 Astronomical Unit (au) away, and 1 au from the Sun and at a zero phase angle. ((NASA NEO Basics Glossary, 2017)

Laboratory (JPL), as part of the WISE mission. NEOWISE uses the WISE satellite, launched in December 2009, to take measurements of asteroids and comets. In its initial phase from December 2009 to September 2010, NEOWISE provided infrared detections of 158,000 asteroids setting limits on numbers, sizes, orbits, and probable compositions, 34,000 of which were new discoveries. (Mainzer et. al., 2011)

The International Asteroid Search Collaboration (IASC), founded by Dr. Patrick Miller of Hardin-Simmons University in October 2006, is an asteroid search campaign and educational outreach programs for high schools and colleges. IASC uses observations from several sky surveys, including Pan-Starrs (Panoramic Survey Telescope and Rapid Response System) and Catalina Sky Survey to find previously undiscovered asteroids. IASC engages more than 3,000 high school students from over 40 countries to analyze images to search for asteroids. Initial discoveries are reported to MPC and confirmed with follow up observations.

Lincoln Near-Earth Asteroid Research (LINEAR) from Massachusetts Institute of Technology, uses a pair of Ground-based Electro-Optical Deep Space Surveillance (GEODSS) telescopes in Socorro, New Mexico, for surveillance of Earth orbiting satellites and detection and cataloguing NEAs. LINEAR is funded by the United States Air Force and NASA. Detected NEAs, comets, unusual objects and main belt asteroids are checked and reported to MPC for designation. As of September 15, 2011, LINEAR reported 30,446,690 observations to MPC consisting of 7,380,528 total detections with 231,082 new discoveries. These discoveries included 2,423 NEOs and 279 comets. (LINEAR, 2013)

The Near-Earth Asteroid Tracking (NEAT) program was a NASA JPL campaign in operation from December 1995 until April 2007 which used two 1.2 meter autonomous



telescopes at Maui Space Surveillance Site and Palomar Observatory to discover and track asteroids larger than 1 km. NEAT was a highly successful survey, discovering more than 40,000 asteroids. ("Minor Planet Discoverers (by number)", 2017)

The Lowell Observatory Near-Earth Object Search (LONEOS), directed by Dr. Ted Bowell and funded by NASA, was a ground based sky survey from 1993 to 2008 covering 20,000 square degrees of observable sky from Flagstaff, Arizona. LONEOS is responsible for the discovery of hundreds of asteroids and reported positional data for millions of asteroid observations to MPC. (Harrington, 2012)

While NASA has been studying NEOs since the 1970s, NASA founded its Planetary Defense Coordination Office in January 2016, which is managed by the Planetary Science Division of the Science Mission Directorate at NASA Headquarters in Washington, D.C. The PDCO leads US government coordination efforts for the planning and response to impact events and is responsible for discovery and tracking of potentially hazardous objects greater than 30 to 50 meters in diameter, which corresponds to objects capable of reaching earth's surface. The PDCO has developed a 5-step plan for impact prevention; 1. Find; 2. Track; 3. Characterization; 4. Deflection Techniques; 5. International Coordination and Education.

### ***Scope of Project***

The monitoring and analysis undertaken in this thesis is part of NASA's OSIRIS-REx mission and Target Asteroids! Campaign. The OSIRIS-REx mission goals includes the first attempt at retrieving samples from the surface of an asteroid. The OSIRIS-REx spacecraft successfully launched from Cape Canaveral on September 8, 2016, beginning

its seven year journey to the asteroid Bennu and back to earth. The mission's primary goals are reflected in the mission's name, Origins Spectral Interpretation Resource Identification Security Explorer (OSIRIS-REx). The mission will give us a better understanding of the origins of planet Earth and the formation of our solar system. Bennu, discovered in 1999 (a.k.a. 1999 RQ36), is approximately 4.5 billion years old, about the same age as earth. Bennu is rich in carbon, a key element in organic molecules. The OSIRIS-REx craft contains two high resolution spectrometers for spectral interpretation of the body and comparison with ground based spectroscopic observations. The mission will also explore the viability of asteroid mining as a source of valuable resources. As reflected in regolith explorer, the mission will gather information about the surface features of asteroid bodies.

The security goals of the mission are the primary focus of this thesis. Asteroid Bennu, at 580 meters in diameter (about the size of six football fields), is one of the most potentially hazardous asteroids known, posing a relatively high risk of impact in the late 2100s. As a sub-mission of the OSIRIS-REx project, NASA launched the Target Asteroids campaign which calls for the observation and extended analysis of known potentially hazardous asteroids for characterization and assessment of risk associated with these bodies. The program targeted specific NEAs and PHAs, calling for professionals and amateur astronomers alike to submit observations of the targeted asteroids for further analysis. These observations are vital to filling in the sparse coverage of these bodies. Greater observational coverage provides more accurate orbit projections and greater precision in the determination of parameters such as rotation period, size, and composition which are important to risk assessment and impact mitigation.

### *Asteroid Characteristics & Characterization*

Like all other solar system bodies, asteroids have elliptical orbits. The first task in determining an asteroid's potential risk of impact is determining its orbital path. This means finding the body's orbital parameters: eccentricity, semi-major axis, perihelion distance, aphelion distance, and inclination angle. The orbital eccentricity ( $e$ ) is a value from zero to one, indicating the degree to which the body's orbital path deviates from a circular path, with zero being a perfect circular orbit and one representing a parabolic orbit. The asteroid's semi-major axis length ( $a$ ) represents the mean distance between the asteroid and sun. The perihelion distance ( $q$ ) and aphelion distance ( $Q$ ) give the asteroid's minimum distance from the sun and maximum distance from the sun, respectively. The inclination angle ( $i$ ) is the angle the asteroid's orbit is inclined with respect to a reference plane. The reference plane for asteroids and other solar system celestial bodies is the orbital plane of earth around the sun. Another important orbital parameter is the orbital period, the time it takes the asteroid to make one complete revolution around the sun. The orbital period is measured in days or years with respect to earth's orbital period.

In addition to being classified by their position in the solar system (i.e. main-belt, Trojan), NEAs are classified by their orbital path with respect to earth's orbital path, perihelion distance and semi major axis. NEA orbital paths are divided into four categories: Apollo, Amor, Aten, or Atira. Each of these orbital classifications are described in Figure 3. (NEO Basics, 2017) From a search of JPL's Small Body Database, the breakdown of the number of known NEAs and PHAs by orbit type are shown in Figure 4. Apollo asteroids are the most abundant NEAs with orbits that cross earth's orbit. Atira type asteroids are

more difficult to detect, having orbital paths that lie completely with earth's orbit, thus fewer asteroids of this type are known (Table 1).

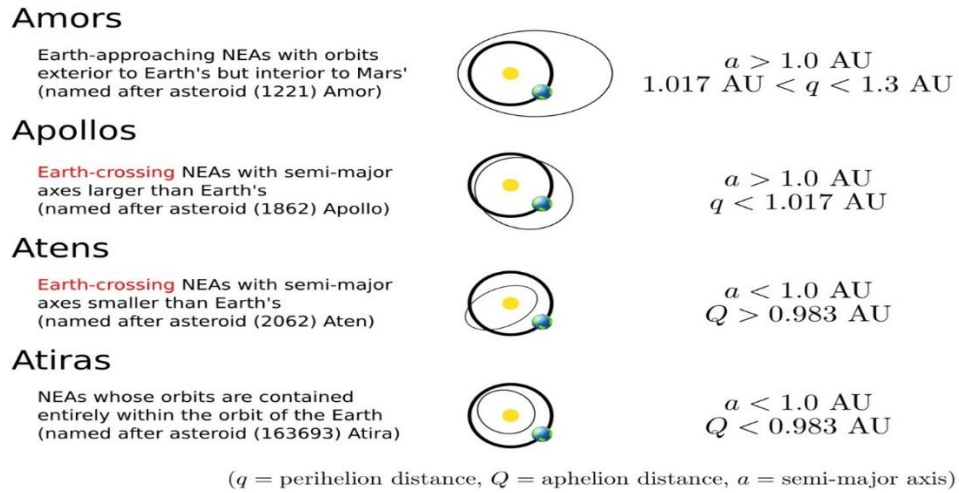


Figure 3: Asteroid orbital classifications (NEO Basics, 2017)

Orbit Type	Number of NEAs	Number of PHAs
<b>Apollo</b>	9,122	1,564
<b>Amor</b>	6,476	104
<b>Aten</b>	1,238	165
<b>Atira</b>	16	5

Table 1: Number of known near earth asteroids and potentially hazardous asteroids per orbit type

The next important step in assessing the impact risk is characterization of the asteroid to determine physical properties of the body. Characterization refers to the determination of size, shape, rotation, and physical composition of the body. These parameters are determined via photometry and spectroscopy.

The reduced magnitude (H) of an object represents how bright an object would appear on a standard magnitude scale at a distance of one astronomical unit at a phase angle of zero degrees. An important parameter of asteroids is the body's albedo, which represents the fraction of incident light that is reflected from the surface of the object. Albedo is a numerical value between zero and one, with one being a perfect reflector and zero representing complete absorption. The diameter of an asteroid is directly related to the albedo and absolute magnitude of the asteroid by the equation:

$$(1) \quad D = \frac{1329}{\sqrt{p}} 10^{-0.2H},$$

where D=diameter, p=albedo, H=reduced magnitude

Asteroid composition is largely determined by the body's spectral characteristics. The most commonly used spectral classification is the Tholen classification system developed by David J. Tholen, originally proposed in 1984. Tholen's classification scheme consists of main types, with types having subclasses. Asteroid spectral type is assigned based on the observed emission spectrum, color, and albedo. According to Tholen's scheme, the majority of asteroids fall into one of the three major types: C-group, S-type, or X-group. The rest of the classification groups encompass smaller type asteroids (A, D, T, Q, R, V-types). Among the more populated groups, C group asteroids are dark carbonaceous bodies. C group is subdivided into B, F, G, and C-types based on specific emission spectra features and albedo. S-type asteroids are siliceous bodies, sometimes referred to as the "stony" asteroids. X-group asteroids are mostly metallic bodies subdivided into three categories: M, E, or P-type. Xm type asteroids are metallic asteroids usually composed mostly of nickel iron. Xe type asteroids are metallic asteroids with high

albedo, while Xp type asteroids are metallic asteroids with low albedo.(Tholen 1984) Another commonly used spectral classification system is the Small Main-Belt Asteroid Spectroscopic Survey (SMASS), developed by Bus and Benzel in 2002 using a survey of 1,447 asteroids. With higher resolution spectroscopy, SMASS was able to resolve narrow emission features leading to more classification subdivisions within the general Tholen taxonomy, while keeping the same three broadest categories.

### ***Rotation Period & Structural Classification***

Asteroids exhibit periodic rotation. The rotation period can be determined from photometric measurements of observations which are used to produce a light curve for the object reflecting variations in apparent brightness as a function of time resulting from the spin of the asteroid about a central axis. The spin behavior of the body is determined by the structure of the asteroid. Symmetrical bodies will exhibit rotation about a single primary axis while more complex shaped bodies will exhibit “tumbling” behavior. In addition to general shape, asteroid structures can be described in two categories, monolithic or rubble piles. Monolithic bodies consist of a single structural mass held together by its own tensile strength. Rubble pile asteroids consist of multiple gravitationally bound bodies, regolith, and dust. The rotation rate of rubble pile asteroids is limited by the so called “spin barrier”, the point at which the centrifugal force from the rotation of the body exceeds the gravitational force holding the system together. Although not structurally sound, rubble pile asteroids typically have some degree of cohesion. The spin barrier has been found to be around 2.2 hours, but can vary with the shape and size of the asteroid. (Hatch et. al. 2015)

### ***Impact Mitigation & Risk Classification***

The risk of impact of a PHA is quantified using the Palermo Scale, calculated based on impact energy, impact probability, and time between current epoch and potential impact. The Palermo Scale is a continuous scale ranging from negative to positive values, with positive values representing cause for concern. A PHA's Palermo Scale value is calculated by the following equations:

$$(2) \quad PS = \log_{10}(R),$$

where R is the relative risk and PS is the Palermo Scale value.

$$(3) \quad R = \frac{P_i}{f_B dT}$$

$P_i$  is the impact probability;  $dT$  is time until impact event in years;  $f_B$  is annual background impact frequency ( $f_B = 0.03 \times E^{-\frac{4}{5}}$ , where E is impact energy in megatons of TNT)

The cumulative Palermo Scale value reflects the seriousness of the entirety of detected potential collision solutions, which includes all potential impact events from a particular body.

$$(4) \quad PS_{cum} = \log_{10} (10^{PS1} + 10^{PS2} + 10^{PS3} + \dots)$$

A Palermo Scale value of less than -2 indicates no risk. A value of -2 to 0 indicates low potential threat and need for monitoring of body. A value greater than zero represents definite cause for concern. (Palermo Technical Impact Scale, 2002) (Chelsey et. al. 2002)

Currently there are 711 NEAs on the NEODyS (Near Earth Objects Dynamic Site) risk list, with the highest values risk associated with asteroid 1950DA with a PS value of -

1.36. There are four bodies categorized as “special” risk: 1950DA, Apophis (PS -3.67), Bennu (PS -2.32), and 2009FD (PS -1.83). (NeoDys Risk List, 2018)

Another commonly used scale to represent the risk associated with an asteroid impact is the Torino Scale, adopted by the IAU in 1999. In contrast to the Palermo Scale, the Torino Scale is a tool used primarily to communicate impact hazard risks to the public. The Torino Scale is a 0 to 10 scale that describes the likelihood and consequences of an impact event but does not consider the time until impact. A body’s Torino Scale Value is calculated from the object’s kinetic energy and probability of impact. Figure 4 shows the descriptions of Torino Scale values. Figure 6 shows the relation between kinetic energy of potentially impacting body and the probability of impact in Torino Scale value assignment. (Morrison et. al. 2004)

**THE TORINO SCALE**

<b>0</b>	<b>ZERO OR VIRTUALLY ZERO CHANCE OF IMPACT</b>
<b>1</b>	<b>IMPACT EXTREMELY UNLIKELY, MERITS MONITORING</b>
<b>2</b>	<b>IMPACT VERY UNLIKELY</b>
<b>3</b>	<b>CLOSE ENCOUNTER WITH AT LEAST 1% CHANCE OF LOCAL DESTRUCTION</b>
<b>4</b>	<b>CLOSE ENCOUNTER WITH AT LEAST 1% CHANCE OF REGIONAL DESTRUCTION</b>
<b>5</b>	<b>CLOSE ENCOUNTER WITH SIGNIFICANT THREAT OF REGIONAL DESTRUCTION</b>
<b>6</b>	<b>CLOSE ENCOUNTER WITH SIGNIFICANT THREAT OF GLOBAL CATASTROPHE</b>
<b>7</b>	<b>CLOSE ENCOUNTER WITH EXTREMELY SIGNIFICANT THREAT OF GLOBAL CATASTROPHE</b>
<b>8</b>	<b>CERTAIN COLLISION WITH LOCAL DESTRUCTION</b>
<b>9</b>	<b>CERTAIN COLLISION WITH REGIONAL DEVASTATION</b>
<b>10</b>	<b>CERTAIN COLLISION CAUSING GLOBAL CLIMATIC CATASTROPHE</b>

*Figure 4: The descriptive Torino Scale.*



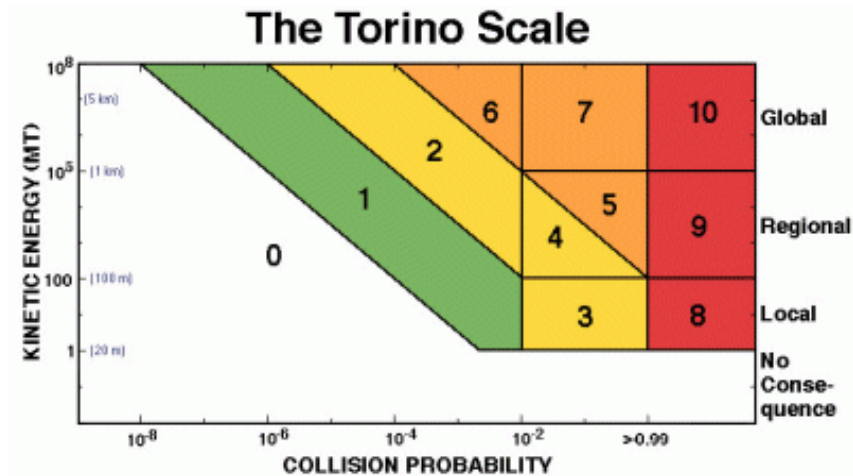


Figure 5: Torino Scale value by kinetic energy and collision probability with geographical effects considered.

JPL’s Sentry System is an automated collision monitoring system which scans current asteroid catalog data for potential impact events over the next 100 years. The Sentry Risk Table is publicly accessible at <https://cneos.jpl.nasa.gov/sentry/>. Objects are added or removed as more observational data becomes available. (Chamberlin et. al. 2001) According to NASA’s Planetary Defense Coordination Office, the highest risk of impact is posed by asteroid 2009FD with a 1 in 714 chance of impact in the year 2185. (Planetary Defense Frequently Asked Questions, 2017)

The strategic planning of mitigation procedures in the event of an impact depends on several key factors including time window until impact, anticipated magnitude of impact, and projected site of impact. Interception of the impacting body is ideal but depends on a substantial length of time from detection to impact. Asteroids cannot simply be “shot down” due to the body’s high velocity. Currently we do not have any tested viable methods to intercept an asteroid on a crash course with our planet. Several potentially viable methods have been proposed, but extensive further research and development is

needed to determine the plausibility of such techniques. A device called a gravity tractor has been proposed in the event of an extended period of time between detection and impact. This method consists of sending a spacecraft to rendezvous with the asteroid in space. The craft would maintain a position close to the asteroid for an extended period of time with the goal of utilizing the gravitational field of the spacecraft to slowly change the trajectory of the asteroid enough so that it passes safely by earth. A similar method is the laser ablation technique in which a spacecraft equipped with a high powered laser would travel to the asteroid then use the laser to chip away fragments of the asteroid body, in turn changing the body's trajectory enough to avoid impact with earth. Another proposed space rendezvous type method is kinetic impact deflection in which a spacecraft would crash into the oncoming asteroid with enough energy to change the body's course. There is also the possibility of using nuclear weapons to change an asteroid's course. The aforementioned methods are still in the development stages and considered future technologies. In any scenario, the longer the window of time, the better the chance of successful interception.

### **Targets Background**

Eight targets from the Target Asteroids! Campaign have been chosen for in-depth study in this work of body characteristics, rotation period, structure, and composition. These targets were chosen specifically for their unique highly varying characteristics to accurately represent the diversity and complex nature of PHAs.

### ***Phaethon***

Asteroid 3200 Phaethon, (aka 1983 TB), is an Apollo type NEA discovered October 11, 1983 by IRAS (Green & Kowal, 1983). Phaethon's name comes from Greek myth of

Phaethon, son of the god Helios, chosen due its close approach to the sun; closer than any other named asteroid. This body involves the Phaethon – Geminid stream complex with orbital elements: eccentricity  $e=0.89$ , semi major axis  $a=1.27$  au, and perihelion distance  $q=0.014$  au. Phaethon exhibits a significant Yarkovsky effect, a gained torque from the absorption and re-emission of heat from sunlight, resulting in the acceleration or deceleration of rotation rate depending on the direction in which reemitted heat is radiated. (Polishook, 2017). Phaethon also exhibits relativistic perturbations due to its close approach to the sun. Historically, Phaethon has been regarded as an extinct cometary nucleus. An alternate theory presented by (deLeon et. al. 2000) suggests Phaethon evolved as a chip off of main belt asteroid (2) Pallas. Weak cometary activity was detected in 2009, 2010, 2012, and 2016, classifying Phaethon as an active asteroid (Jewitt & Li, 2010; Li & Jewitt, 2013; Jewitt et.al. 2013; Hue & Li, 2017).

Phaethon is a B/F type asteroid and is the largest of all known near sun asteroids with a diameter of  $5.1\pm 0.2$  km (absolute magnitude: 14.6) (Hanus et. al. 2016). It has a low geometric albedo at 0.1066 and an orbital period of 523.5025 days, or 1.43 earth years (JPL small body database). Phaethon has a minimum orbit intersection distance of 0.0194544 au and will have a close approach with earth on December 16, 2017 at 05:46 UT at 0.0689315504 au.

### *Icarus*

(1566) Icarus was discovered June 27, 1949 by Walter Baade at Palomar Observatory. Icarus has an Apollo type orbit and like Phaethon, it is a near sun asteroid. It was named for Icarus of Greek mythology known for flying too close to the sun. With a perihelion distance ( $q$ ) of 0.1866902 au, it is one of the closest approach near sun asteroids

known and has a highly eccentric orbit ( $e=0.82681$ ). Icarus exhibits strong relativistic perturbations due to its close approach to the sun.

Spectral observations classify Icarus as a Q-class stony asteroid with a very high albedo of 0.51. Icarus has a semi-major axis ( $a$ ) of 1.077946 au, orbital inclination ( $i$ ) of 22.85205 degrees, and aphelion distance ( $Q$ ) 1.9620157 au. Icarus has an orbital period of 408.783979 days (1.12 years) and MOID of 0.035204 au. Icarus is a rapid rotator with previously published rotation period of 2.2726 hours (Warner et.al. 2009) and a diameter of 1.27 km (Harris 1998).

### ***Hathor***

Upon its discovery on October 22, 1976 by C.T. Kowal at Palomar Observatory, 2340 Hathor was among the smallest asteroids known at the time with a diameter estimate of just 0.3 km based on its absolute magnitude of 20.2. However, Spitzer Space Telescope measurements yield an unusually high albedo of 0.6 (Thomas et. al. 2010), uncharacteristic of Hathor's Sq type spectral classification. Since original size calculations were based upon medium albedo (0.15) assumptions, evidence suggest Hathor may be as small as 170 meters in diameter. Hathor has the following orbital parameters: eccentricity ( $e$ ) 0.4498842, semi-major axis ( $a$ ) 0.843829246 au, perihelion distance ( $q$ ) 0.46420383 au, aphelion distance ( $Q$ ) 1.223455 au, inclination ( $i$ ) 5.854591 degrees, and an orbital period of 283.1263477 days (0.78 years). Hathor has an MOID of 0.00687373 au. Previous work by Warner et. al. (2009) gives a rotation period of 3.350 hours.

## ***Bede***

3691 Bede, an Amor type asteroid, was discovered March 29, 1982 by L.E Gonzalez and Cerro El Roble. It was named after the historical figure “The Venerable Bede”, known as the “Father of English History”. Bede is a spectral type Xc asteroid (Xu et. al. 1995; Bus & Binzel 2002) with extraordinarily high albedo of  $0.593 \pm 0.120$ . (NEOWISE 2011) Previous size calculations, based on medium albedo of 0.15 and absolute magnitude 14.7, gave a diameter estimate of 4.3 km; however, this is likely too large given the measured high albedo. Bede has an MOID of 0.352538 au and a period of 863.2774835 days (2.36 years). Bede’s primary orbital elements are: eccentricity  $e=0.28431627$ , semi-major axis  $a=1.7743311$  au, perihelion distance  $q=1.2698599$  au, aphelion distance  $Q=2.278802$  au, and inclination angle  $i=20.360489$  degrees.

Bede has an unusually long rotation, previously estimated at 226.8 hours (Warner et. al. 2009), suggesting a rubble pile structure.

## ***2004 JN 13***

Apollo asteroid 2004 JN13 (aka 214088) was discovered May 15, 2004 by LINEAR at Socorro. Orbital elements from JPL’s small body database are as follows: eccentricity  $e=0.6926766159$ , semi-major axis  $a=2.88901672$  au, perihelion distance  $q=0.8878624$  au, aphelion distance  $Q=4.89017104$  au, inclination  $i=13.29513289$  degrees, and long orbital period of 1793.5913874 days (4.91 years). It has an MOID of 0.131387 au. 2004 JN13 has an absolute magnitude of 15.3 and a rotation period of 6.342 hours (Warner et. al. 2009). It has a measured diameter of  $2.423 \pm 0.058$  km and an albedo  $0.250 \pm 0.031$  (NEOWISE).

### ***2002 FG7***

2002 FG7 (aka 141527) is an Apollo asteroid discovered March 28, 2002 by NEAT at Haleakala. It has an orbital period 680.285436 days (1.86 years), absolute magnitude 18.9, and MOID 0.042096 au. Previous analysis of light curves gives a rotation period of 6.306 hours (Warner et. al. 2009). JPL's small body database gives the following orbital elements: eccentricity  $e=0.62686787775$ , semi-major axis  $a=1.51377675$  au, perihelion distance  $q=0.56483873$  au, aphelion distance  $Q=2.46271477074$  au, and orbit inclination  $i=9.20752503$  degrees.

### ***2004 QQ***

Apollo asteroid 2004 QQ (aka 175114) was discovered August 17, 2004 by the LINEAR survey at Socorro. It has an absolute magnitude of 16.6 and the following orbital elements: eccentricity  $e=0.66344725$ , semi-major axis  $a=2.2500745$  au, perihelion distance  $q=0.75726876$  au, aphelion distance  $Q=3.7428803$  au, inclination angle  $i=5.722791095$  degrees, and an orbital period of 1232.80326893 days (3.38 years). (JPL Small Body Database). 2004 QQ has a previously determined rotation period of 8.879 hours (Warner et. al. 2009) and an MOID of 0.0599394 au.

### ***2004 BL86***

Discovered January 30, 2004 by LINEAR at Socorro, 2004 BL86 (aka 357439) is an Apollo type asteroid with an absolute magnitude of 19.3. This asteroid has the following orbital parameters: eccentricity  $e=0.40259709$ , semi-major axis  $a=1.50222404$  au, perihelion distance  $q=0.897433$  au, aphelion distance  $Q=2.107015072$  au, inclination angle

23.7750615 degrees and orbital period 672.51269976 days (1.84 years). It has an MOID of 0.00924442 au.

2004 BL86 is a binary asteroid with a fast rotation period of 2.6205 hours (Warner et. al. 2009).

## Chapter 2

### Data & Methods

#### *Target Asteroids Observations*

Observations obtained via NASA's Target Asteroids! Campaign were calibrated by the contributing observer. Requirements for contributing observers were access to a minimum 8 inch telescope equipped with CCD camera. Photometry was performed on all viable images using the MPO Canopus software.

#### *RCT Observations*

Additional observations for certain targets were obtained via Western Kentucky University's Robotically Controlled Telescope (RCT) located in Kitt Peak, Arizona. The RCT is a 1.3-meter (50inch) f/14 Cassegrain telescope equipped with 2048×2048 pixel SITe CCD camera. Images were flat field and bias corrected using the IRAF astronomical software package. Photometry was performed using the MPO Canopus software.

#### *ALCDEF Photometry Database*

Available photometry data for each target was downloaded from the publicly accessible Asteroid Light Curve Photometry Database (ALCDEF) photometry database in order to extend the length of the available time series. Table 2 gives a breakdown of number of observations for each target by source and observed band.



	<b>Target Asteroids</b>	<b>RCT</b>	<b>ALCDEF</b>	<b>Bands</b>	<b>Totals:</b>
<i>2002 FG7</i>	21	0	1,864	B,V,R,I	<b>1,885</b>
<i>2004 BL86</i>	0	0	1,776	R	<b>1,776</b>
<i>2004 QQ</i>	131	0	0	V,R	<b>131</b>
<i>2004 JN13</i>	23	0	1,187	B,V,R,I	<b>1,210</b>
<i>Bede</i>	1,005	182	0	V,R	<b>1,187</b>
<i>Hathor</i>	99	0	1,303	C,B,V,R,I	<b>1,402</b>
<i>Icarus</i>	84	0	2,527	B,V,R,I	<b>2,611</b>
<i>Phaethon</i>	18	594	896	V,R	<b>1,508</b>
<b>Totals:</b>	<b>1,381</b>	<b>776</b>	<b>9,553</b>		<b>11,710</b>

*Table 2: Number of observations per target from Target Asteroids, the Robotically Controlled Telescope, and the ALCDEF Asteroid Photometry Database.*

### **Data Processing**

Instrumental magnitude values derived from photometry were corrected for atmospheric extinction, position in orbit, and phase angle. All needed parameters were also obtained from JPL Horizon’s ephemeris generator including phase angle ( $\alpha$ ), observer to sun distance (R), observer to target distance (D); and extinction. The magnitude corrected for the position in orbit was calculated using the following equation:

$$(5) \quad V_R = V - 5\log(RD)$$

where V is observed (photometric) magnitude; R is distance between sun and asteroid (AU); D is distance between earth and asteroid (Buchheim 2010).

Magnitude adjustments for phase angle were calculated according to the Standard Phase Curve Model (H-G Model) as described in Buchheim 2010

$$(6) \quad H(\alpha) = H_0 - 2.5 \log[(1 - G)\Phi_1(\alpha) + G\Phi_2(\alpha)]$$

Where  $H_0$  is the reduced magnitude at 0 phase angle, (sun,-target-observer angle) ( $\alpha=0$ );  $\alpha$  is the solar phase angle;  $G$  is the slope of the phase curve<sup>1</sup>;  $\Phi_1$  and  $\Phi_2$  are functions defining the scattering at the surface of the asteroid. <sup>1</sup> $G$  is the slope of the best fit line of the plot of  $H$  vs  $\alpha$ . If the data is insufficient to determine  $G$ ,  $G$  is assumed to be a standard value of 0.15. (Buchheim 2010)

*Single & Multiple Scattering Equations*

$$(7) \quad \Phi_1(\alpha) = W\phi_{1S} + (1 - W)\phi_{1L}$$

$$(8) \quad \Phi_2(\alpha) = W\phi_{2S} + (1 - W)\phi_{2L}$$

$$(9) \quad W = \exp[-90.56 \tan^2(\frac{\alpha}{2})]$$

$$(10) \quad \phi_{1S} = 1 - \frac{C_1 \sin(\alpha)}{0.119 + 1.341 \sin(\alpha) - 0.754 \sin^2(\alpha)}$$

$$(11) \quad \phi_{1L} = \exp[-A_1 (\tan \frac{\alpha}{2})^{B_1}]$$

*Constants for Equations 7 & 8:*

$$A_1 = 3.332; B_1 = 0.631; C_1 = 0.986$$

$$(12) \quad \phi_{2S} = 1 - \frac{C_2 \sin \alpha}{0.119 + 1.341 \sin \alpha - 0.754 \sin^2 \alpha}$$

$$(13) \quad \phi_{2L} = \exp[-A_2 (\tan \frac{\alpha}{2})^{B_2}]$$

*Constants for Equations 9 & 10*

$$A_2 = 1.862; B_2 = 1.218; C_2 = 0.238$$

Uncertainties on final derived magnitudes were calculated according to standard error propagation procedure. Parameters obtained from JPL Horizons ephemeris generator were taken to have 99.7% accuracy per database statement.

## Chapter 3

### Analysis

Variations in the corrected observed brightness of an asteroid as a function of time, known as a light curve, can be used to determine the rotation period of the asteroid. There are various methods of time series analysis used to extract periodic signals with a body's light curve, each having unique advantages and disadvantages. For this thesis, the Lomb-Scargle periodogram method was chosen for rotation period analysis due to its usefulness in extracting periodic signals in unevenly sampled time series data. The Lomb-Scargle method is a variation of the discrete Fourier transform rigorously described by Van der Plas. (VanderPlas 2017). The following section is a general summary of the main points of the Lomb-Scargle periodogram.

#### *Lomb-Scargle Time Series Analysis*

Classical Fourier based methods are commonly used to extract periodic signals.

#### *Continuous Fourier Transform*

$$(14) \quad \hat{g}(f) = \int_{-\infty}^{\infty} g(t)e^{-2\pi ift} dt$$

where  $f$  is frequency,  $t$  is time, and  $g(t)$  is a continuous function to be transformed. Since the data to be analyzed comes in the form of discrete samples, the discrete form of the Fourier transform is more useful.

## Discrete Fourier Transform

$$(15) \quad \hat{g}(f) = \sum_{n=0}^N g_n e^{\frac{-2\pi i f_n \Delta t}{N}}$$

where the relevant frequency range is  $0 \leq f \leq \frac{1}{\Delta t}$ , and

$$(16) \quad g_n = g(n\Delta t)$$

This method is sufficient if the data samples are evenly spaced; however, given the nature of astronomical observations, this is often not the case. For the treatment of unevenly spaced time series data sets, the Lomb-Scargle periodogram was developed. (Lomb 1976; Scargle 1982) This algorithm is a Fourier-based method with characteristics of the least squares method. (VanderPlas 2017) The Lomb-Scargle method is given by:

$$(17) \quad P_{LS}(f) = \frac{1}{2} \left\{ \frac{(\sum_n g_n \cos(2\pi f [t_n - \tau]))^2}{\sum_n \cos^2(2\pi f [t_n - \tau])} + \frac{(\sum_n g_n \sin(2\pi f [t_n - \tau]))^2}{\sum_n \sin^2(2\pi f [t_n - \tau])} \right\}$$

where  $\tau$  is specified for each frequency to ensure time-shift variance:

$$(18) \quad \tau = \frac{1}{4\pi f} \tan^{-1} \left( \frac{\sum_n \sin(4\pi f t_n)}{\sum_n \cos(4\pi f t_n)} \right)$$

The uncertainty in the peak location for a particular frequency in the Lomb-Scargle periodogram can be estimated as:

$$(19) \quad \sigma_f \approx f_{1/2} \sqrt{\frac{2}{N\epsilon^2}}$$

where  $f_{1/2}$  is the half-width at half-max of the peak;  $N$  is the number of samples; and  $\epsilon$  is the average signal to noise ratio of the samples.

Another useful feature of the Lomb-Scargle periodogram is its ability to give the probability that a peak is a false alarm. For a particular peak in the periodogram, the False Alarm Probability can be estimated by (Independent Frequency Method) (VanderPlaas 2017):

$$(20) \quad FAP(Z) \approx 1 - [P_{single}(Z)]^{N_{eff}}$$

where  $P_{single}$  is the cumulative probability of observing a periodogram value less than  $Z$  in data consisting only of Gaussian noise (VanderPlaas 2017).

$$(21) \quad P_{single}(Z) = 1 - \exp(-Z)$$

Where  $Z$  is the periodogram amplitude at a given frequency  $f$ , and  $N_{eff}$  is the effective number of independent frequencies in the periodogram.  $N_{eff}$  can be estimated as  $N_{eff} \approx f_{max}T$

## ***Light Curve Inversion Techniques***

### ***Convex Inversion***

Photometry and light curve analysis has long been useful tool in determining characteristics of cosmic bodies. Most commonly, time series analysis of fluctuations in brightness is used to determine periodic properties of cosmic bodies, such as rotation period, as outlined in the previous section. In addition to rotation period, the rotation pole direction, scattering parameters, and shape of an asteroid can be derived through a technique called light curve inversion. Aside from observed changes in brightness resulting from changing distance from the observer and sun, the shape of an asteroid body is the most important cause of observed fluctuations in brightness, with albedo effects being

negligible by comparison. It is even possible to separate shape effects from albedo variegation. The light curve inversion process developed by Kaasalainen and Torppa (Kaasalainen et. al 2000, 2001) starts by modeling an asteroid body as a polyhedron with triangular facets known as the convex hull. A facet is a relatively smooth surface area connected to other facets by vertices. The contribution of a surface patch  $ds$  to the total brightness is given by:

$$(22) \quad dL = S(\mu, \mu_0) \omega ds$$

where  $S$  is the first order scattering law and  $\omega$  is albedo.

$$(23) \quad \mu = \vec{E} \cdot \vec{n}$$

$$(24) \quad \mu_0 = \vec{E}_0 \cdot \vec{n}$$

where  $\vec{n}$  is the unit normal vector of  $ds$ ,  $\vec{E}$  is the unit vector in the direction of earth, and  $\vec{E}_0$  is the unit vector in the direction of the sun. The algorithm uses a combination of the Lambert Law,  $S_L = \mu\mu_0$ , and Lommel-Seeliger Law,  $S_{LS} = \frac{S_L}{\mu + \mu_0}$ , to compute the scattering function.

$$(25) \quad S(\mu, \mu_0) = \frac{\mu\mu_0}{(\mu + \mu_0)}$$

Next the program uses an  $N^2$  algorithm employing a ray tracing procedure that checks for vertices above each facet's local horizon and tests for connected facing facets which are blockers of light. Positions of facets and vertices are computed with respect to the local horizon. Facets for which no vertices appear above the local horizon belong to the convex hull. The position of facets at differing angles with respect to adjoining facets

creates non-convexities in the overall structure of the object adequately modeling the non-convexities observed in asteroid structures. Synthetic light curves are computed for the model based on projections along the viewing and illumination axes. For a facet to be visible and illuminated, both  $\mu$  and  $\mu_0$  must be positive. If a facet is particularly large, representing a large portion of the total surface area, a number of test points (few tens of points) on the facet are selected and shadowing is checked for each point separately. Synthetic light curves are compared to observed light curves and positions of facets and vertices are adjusted until fit is optimized through  $\chi^2$  minimization. (Kaasalainen et. al 2000)

To get a stable, accurate model, multiple light curves at different viewing geometries are needed. To improve solutions, available photometric data for each target was downloaded from ALCDEF’s Asteroid Photometry database in addition to Target Asteroid observations and RCT observations. No ALCDEF data was available for asteroid Bede and asteroid 2004QQ. Thus asteroid 2004QQ could not be modeled, however, sufficient RCT data existed to allow modeling of Bede. A summary of number of individual light curve blocks used and phase angle range for each target is given in Table 3.

	<b>Phase Range (degrees)</b>	<b>Number of Light Curve Blocks</b>
<b>2002 FG7</b>	51	27
<b>2004 BL86</b>	65	24
<b>2004 JN13</b>	50	7
<b>Bede</b>	36	12
<b>Hathor</b>	63	26
<b>Icarus</b>	66	50
<b>Phaethon</b>	25	13

*Table 3: Summary of data used in asteroid structure modeling. Note: Asteroid 2004QQ was not modeled due to insufficient data.*



### ***Determination of Pole and Rotation Period***

In order to derive the rotation axis and pole orientation of the asteroid, the necessary vectors must be translated from the ecliptic frame to the frame of the asteroid. This requires the use of a translation matrix,  $R_i(\alpha)$  which transforms the ecliptic vector  $\vec{r}_{ecl}$  to the asteroid's reference frame,  $\vec{r}_{ast}$ , through the following operation:

$$(26) \quad \vec{r}_{ast} = R_z(\varphi_0 + \omega(t - t_0))R_y(\tilde{\beta})R_z(\lambda)\vec{r}_{ecl}$$

Where  $\beta$  is the ecliptic polar angle of the asteroid measured from the positive z axis (range  $[0, \pi]$ );  $\lambda$  is the longitude;  $\omega$  is the angular rotation speed (related to the rotation period by  $\omega = \frac{2\pi}{P}$ ), assumed to always be in the positive direction. The time is given by  $t$  and  $t_0$  is chosen to be when an observed light curve at small solar phase angle is at a minimum. The angle  $\varphi_0$  is set to the azimuthal angle of the vector  $R_y(\tilde{\beta})R_z(\lambda)\vec{r}_{ecl}$ , where  $\vec{r}_{ecl}$  is the direction vector of the earth at time  $t_0$ . This convention for  $t_0$  and  $\varphi_0$  puts the earth in the xz plane and aligns the long axis of the asteroid with the x axis. (Kassalinen et. al., 2001)

### ***Treatment of Data in Period Analysis***

For each target, rigorous rotational period analysis was performed using the Lomb-Scargle method via Python's Astropy package. In cases where sufficient data was available, physical shape modeling was performed using software developed by Kaasalainen (Kaasalainen & Durech, 2018).

## Chapter 4

### Period Determination & Structure Modeling

The following sections will give the results of the period analysis and modeling the shape of the asteroid sufficient data exists. Working with data sets from multiple sources can provide a unique set of challenges and the challenges encountered will also be addressed. Magnitude offsets between data from different sources were calculated by performing a Gaussian fit on peaks to find the maxima given that the maximum magnitude is constant across a complete rotation, then assuming a constant offset throughout data. Zero points for each light curve for calculating phase values were found in a similar manner.

Asteroids present another unique challenge in rotation period analysis: these bodies are often non-spherical and asymmetric. A spherical rotating system produces a light curve that is a sinusoid. Since we are dealing with more complex shapes than what we see with spherical rotating objects, we can expect more complex features in the resulting signal. The resulting tell-tale signs are present in the shape of the object's light curve, often presenting as uneven amplitudes of maxima and asymmetric peaks in the light curve. Period analysis algorithms do not attribute the differences in amplitudes as relating to the period, but rather analyze the location of peaks in period determination. Thus, an algorithm will often return a period result that is half the actual period. This condition is easily discerned when a light curve shows obvious uneven maxima; however this can be missed if the observational data does not cover a full rotation cycle.

In addition, asteroids often have relatively rough surfaces with substantial scattering of reflected light, thus asteroid light curves are typically “noisy”. The importance of high quality expansive data sets becomes apparent when trying to determine information about the body’s structure from these subtle variations. Assumptions must be made as to degree of noise from systematic uncertainty vs variability due to surface roughness.

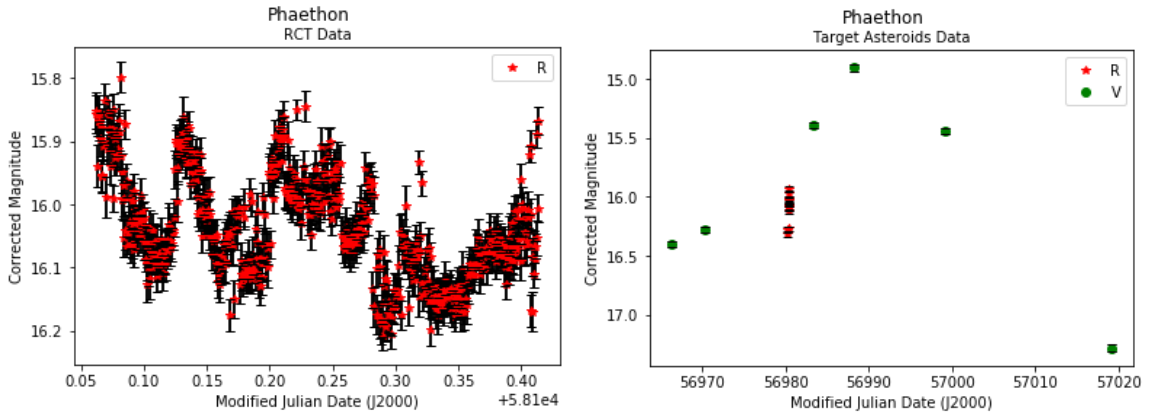
As with analysis of any periodic signal, appropriate sampling is vital to producing reliable results. Sampling is also a very important factor when planning observations as will be evident in the following results. Most asteroids have periods on the order of a few hours to a few days. Accuracy of and confidence in rotation period results is contingent upon having observations that cover at least a full rotation cycle, with coverage of multiple cycles preferred. In most cases, single observations per night over time spans on the order of days or weeks is insufficient to produce accurate rotation period results. In addition, the quantity of data is an important consideration in the reliability of results. The very nature of period analysis ensures more data equals more accurate results. These factors were the biggest challenges to overcome in this thesis - working with fairly sparse data sets at less than ideal sampling rates.

### ***Lomb-Scargle Period Analysis***

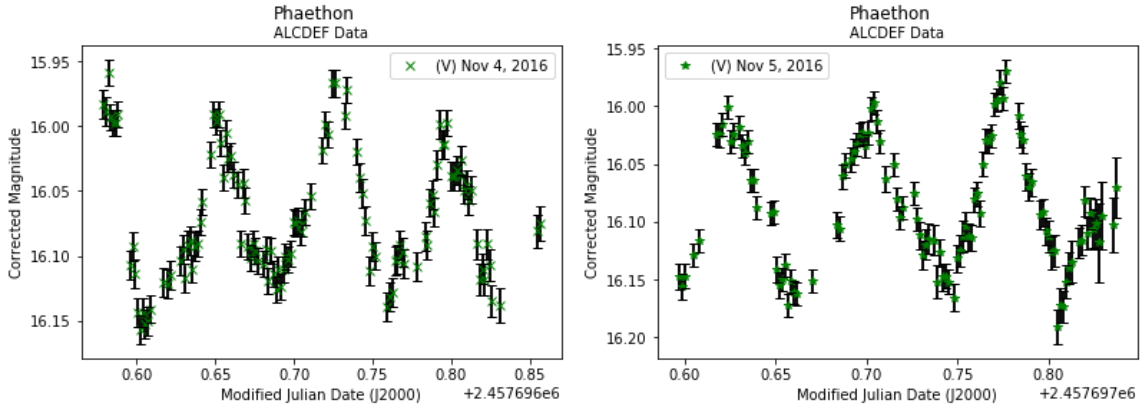
#### ***Phaethon***

Photometric data used for the rotation period analysis for asteroid 3200 Phaethon is presented in Figures 6-9. Observations were obtained using RCT on December 13, 2017, near Phaethon’s time of close approach with earth on December 16, 2017. These observations spanned a continuous period of just over eight hours. The close approach data

yielded an interesting light curve with somewhat unique features (Figure 6). Target Asteroid data for this target was somewhat sparse as seen in Figure 7. Additional photometric data used to supplement data set from ALCDEF shown in Figures 8 and 9.



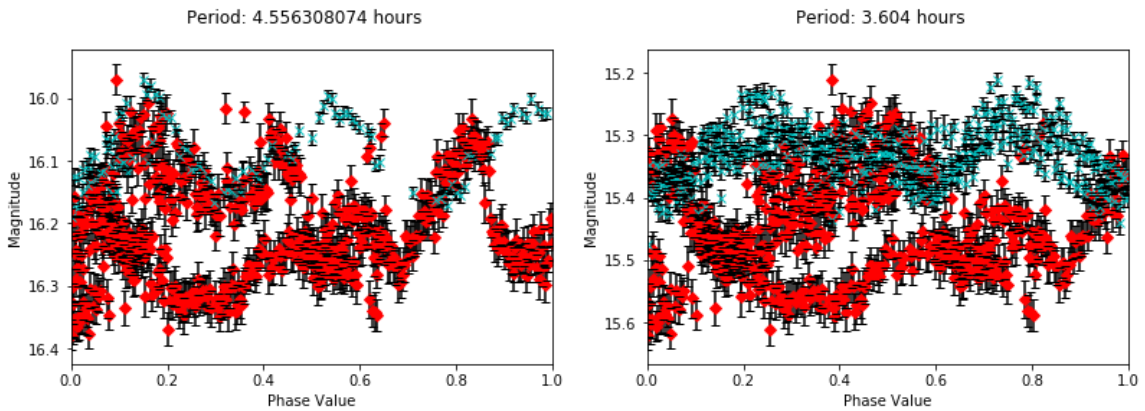
Figures 7-8: Light curves used in period analysis for Phaethon from RCT and Target Asteroids



Figures 8-9: Selected light curves from ALCDEF database used in period analysis for Phaethon.

A period analysis of the RCT data resulted in two possible periods with high confidence factors. One of these corresponded to previously published value of 3.604 hours, with a false alarm probability of  $6.40 \times 10^{-62}$ . Another periodic signal was indicated at 4.556 hours with a false alarm probability of  $7.43 \times 10^{-38}$ . Phase plots encompassing RCT and ALCDEF data sets for both periods are shown in figures 10 and 11. As seen in Figure

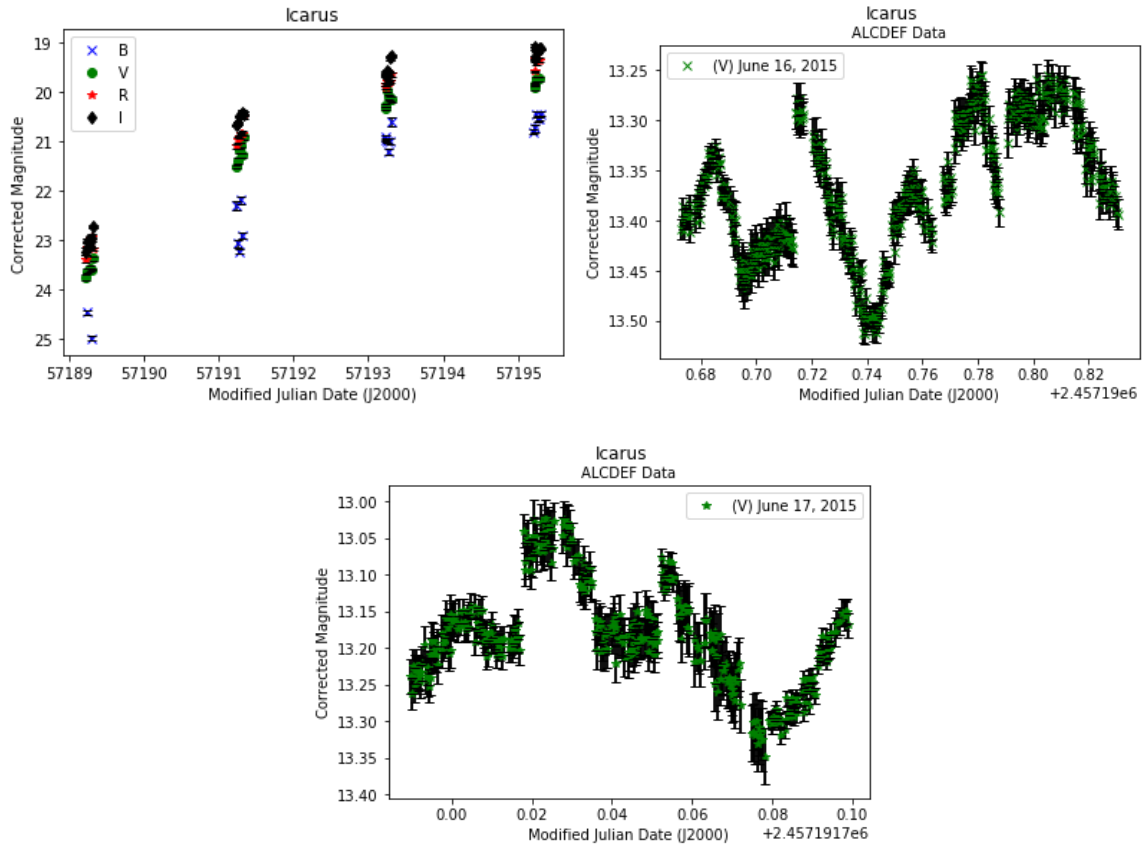
11, the RCT data does not phase with the data from ALCDEF for the previously published period 3.604 hours. Examination of the RCT light curve shows some unexpected variation. This could be a result of the presence of multiple periodicities, which involves a more rigorous analysis to extract which is beyond the scope of this thesis.



*Figures 10 & 11: Phase plots for rotation periods of 4.5563 hours and 3.604 hours. RCT data is displayed as red diamonds and ALCDEF data is displayed as blue x's.*

### ***Icarus***

The photometric data used in the rotation period analysis of Icarus are presented in Figures 12, 13, and 14. Target Asteroid observations consisted of observations in B, V, R, and I bands with two observations per band over a time span of four days. Additional photometric data was obtained from ALCDEF database (Figures 13 and 14) to supplement period analysis.

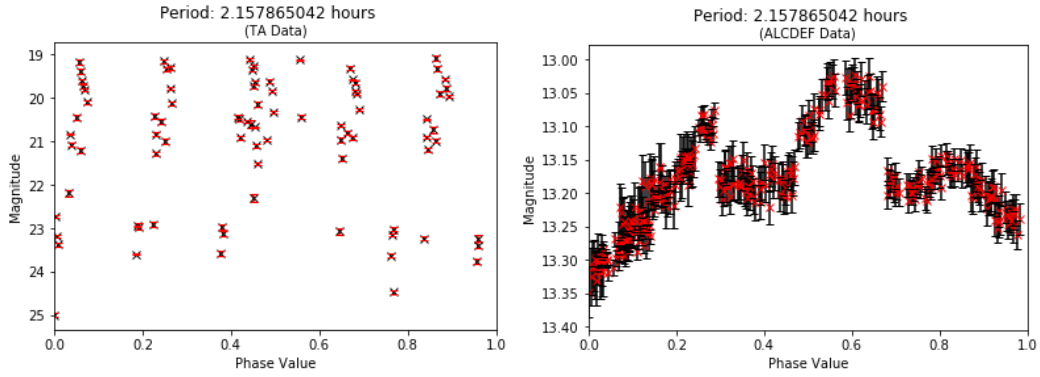


Figures 12 (left), 13 (right) & 14(center): Light curves for TA data and ALCDEF data.

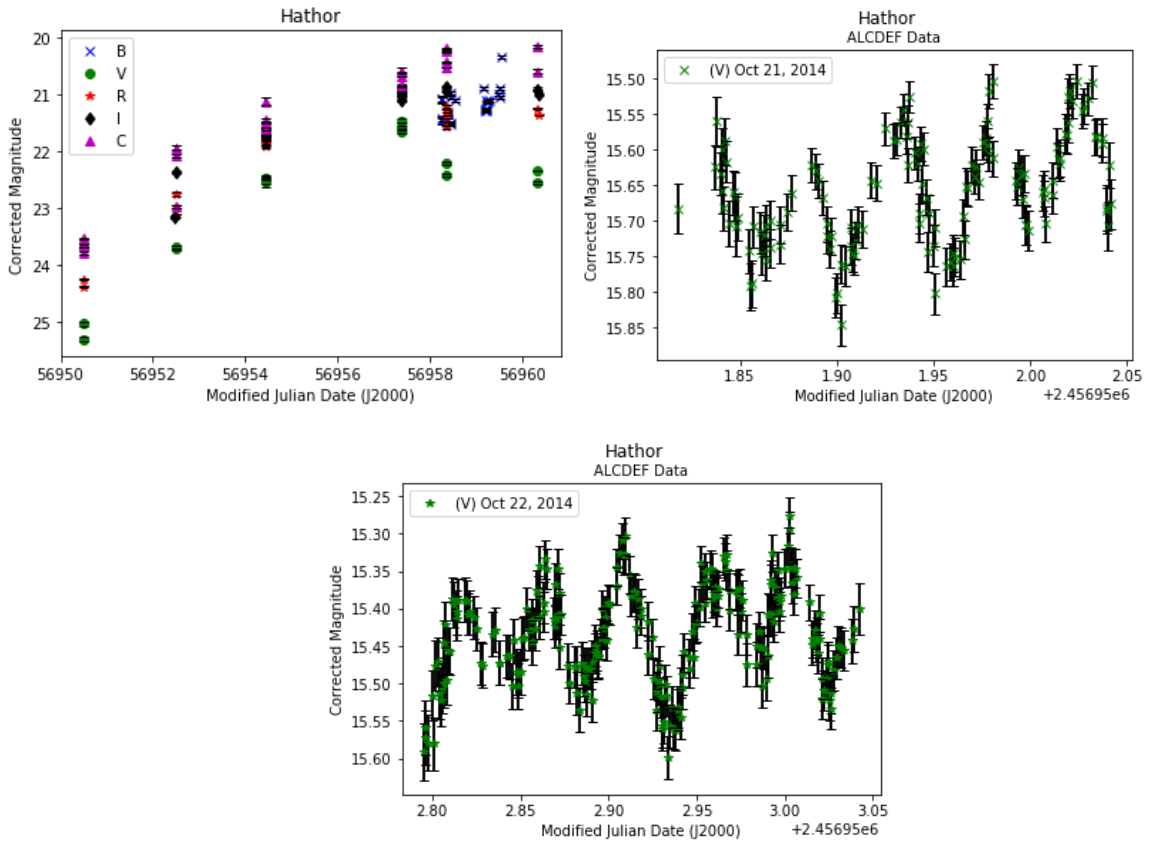
A period analysis of TA data was attempted which gave a period of 2.1579 with a false alarm probability of  $9.44 \times 10^{-22}$ , which is consistent with the published period of 2.2726 given the sparse data set. Phase plots of the resulting period of 2.1579 and the published period of 2.2726 are shown in figures 15 and 16.

### *Hathor*

The Target Asteroids data for Hathor consisted of B, V, R, and I band observations sampled over a period of ten days. The light curve of TA data is shown in figure 17. Additional ALCDEF data used in confirmation of period analysis is shown in figures 18 and 19.

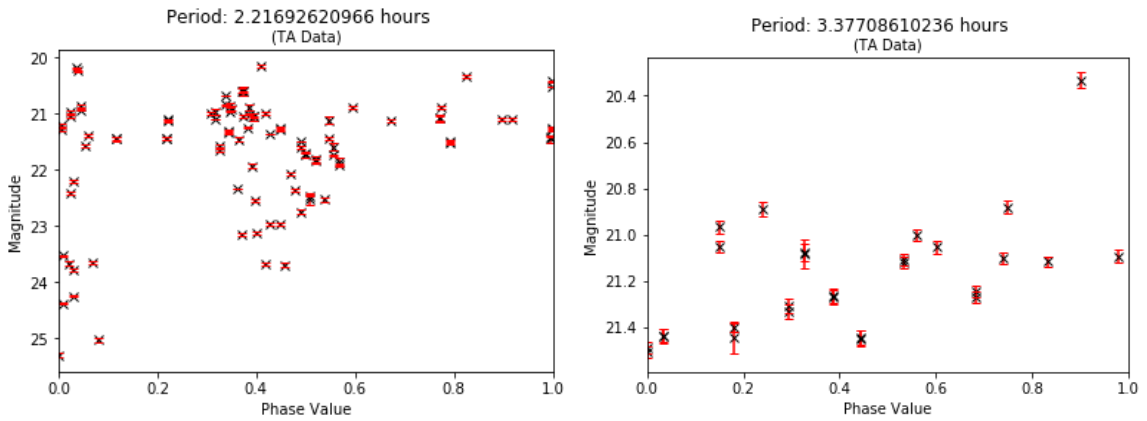


Figures 15 & 16: Icarus phase plots for period of 2.1579 hours for TA data (left) and ALCDEF data (right).

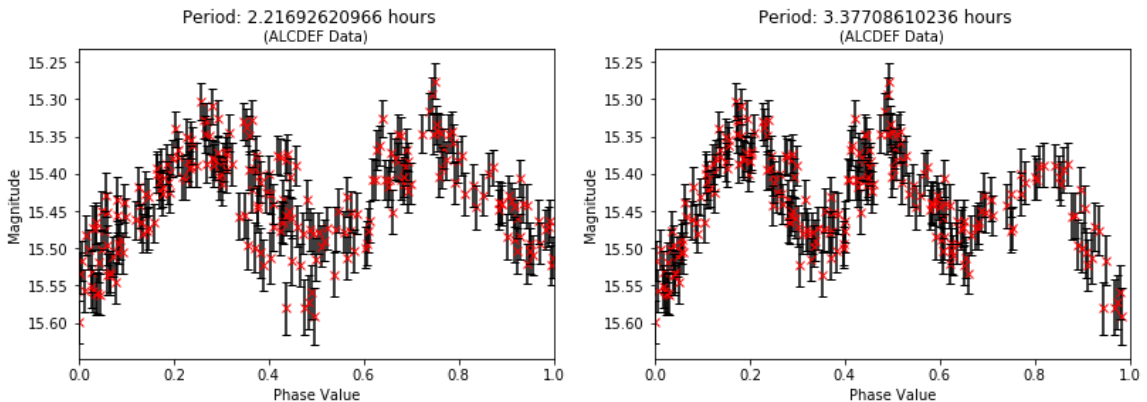


Figures 17 (left), 18 right, & 19 (bottom): Light curves for TA (left) and ALCDEF data (right and center).

A Lomb Scargle analysis indicated probable periods at 3.3771 hours and 2.2169 hours with false alarm probabilities of  $5.28 \times 10^{-16}$  and  $4.98 \times 10^{-46}$  respectively. The 3.3771 hours result in close agreement with published value of 3.350 hours. Phase plots for period 3.3771 hours period produces a tri-modal phase plot. Phase plots for this period are shown in Figures 21, 23, and 25. ALCDEF data fits well with this period; however TA data is not a good but some evidence of corresponding peak locations can be seen in Figures 21 and 25. The TA data phases better with the bimodal period result of 2.2169 hours. ALCDEF data confirms a good fit for this result as seen in Figures 20, 22, and 24.

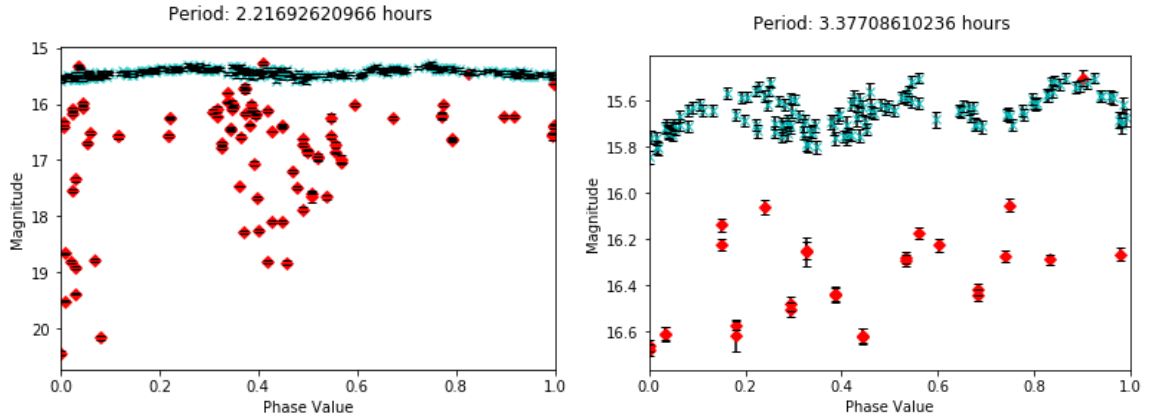


Figures 20 & 21: Phase plots for TA data for periods 2.169 hours and 3.3771 hours.



Figures 22 & 23: Phase plot for ALCDEF data for periods of 2.2169 hours and 3.3771 hours.





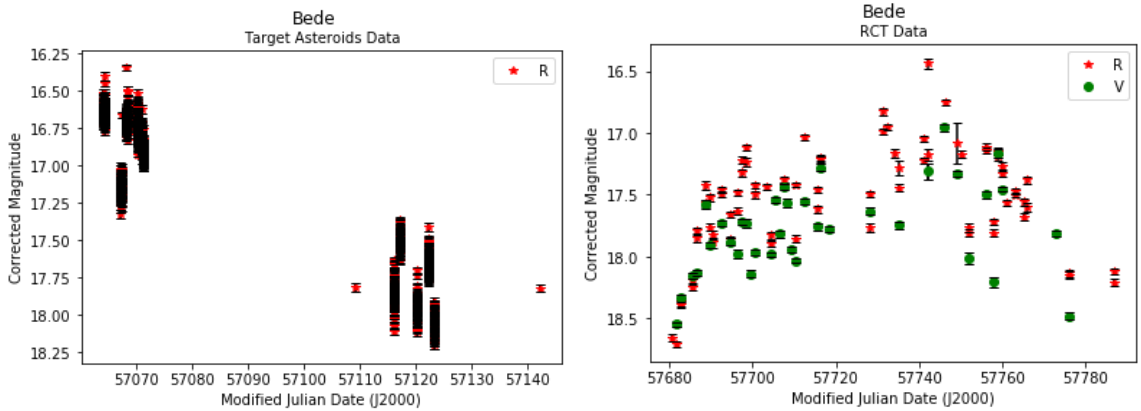
Figures 24 & 25: Phase plots for period 2.169 hours and 3.3771 hours with TA and ALCDEF data, red and blue points, respectively.

### ***Bede***

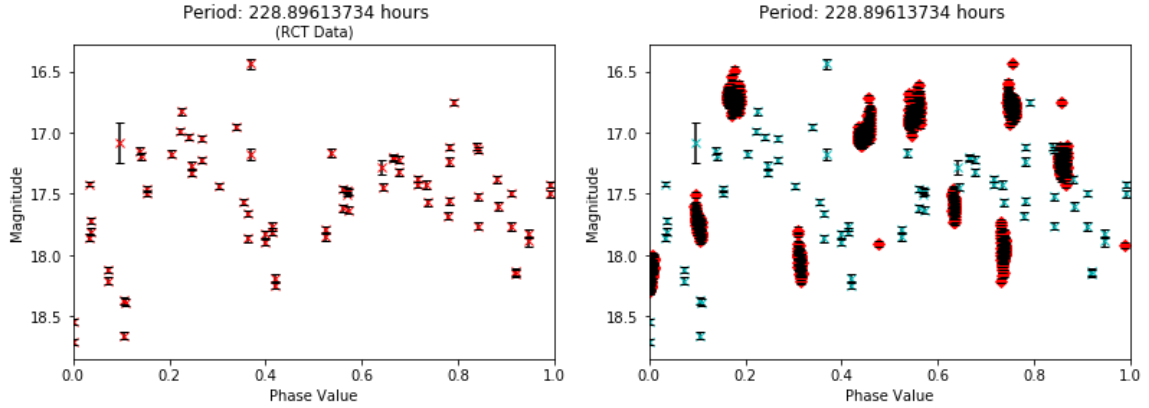
Bede is a somewhat unique asteroid amongst this group of targets having a rotation period on the time scale of days as opposed to a few hours. Long rotation periods are often seen in asteroids with “rubble pile” structures, thus the spin rate is limited in order for the system to remain stable. Bede represents the largest data set of TA data used in this work, with continuous nightly observations obtained ten separate nights over a two month time span. The light curve of TA data is presented in Figure 26. Additional observations were obtained from RCT consisted of single R and V band nightly observations spanning every observable night over a 100 day period. The light curve of RCT data is presented in Figure 27.

Previous work cites the period for Bede at 226.8 hours with a 30% uncertainty due to less than full cycle coverage of observations (Pravec et. al., 2005; JPL Small Body Database, 2018). A Lomb-Scargle period analysis yielded differing results for the TA data and RCT. Analysis of RCT data confirmed the cited period within the stated uncertainty with a result of 228.8961 hours (9.54 days). The phase curve for this result is given in

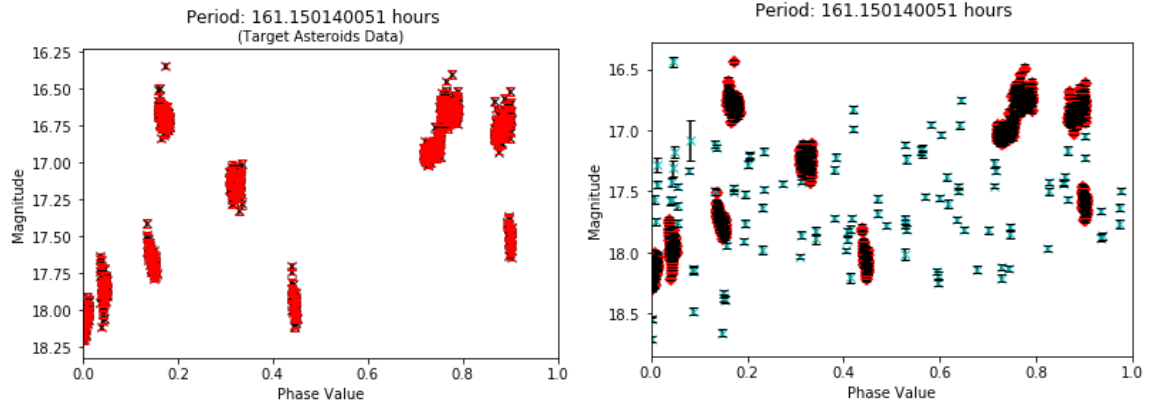
Figures 29 and 31. As seen in Figure 29, the TA data did not fit well with this result. Analysis of TA data gave a rotation period of 161.1501 hours or 6.715 days. Bede is classified as a tumbling asteroid, exhibiting a more complex rotational behavior, thus multiple periodicities are expected to be present.



Figures 26 & 27: Light curves of TA and RCT data for asteroid Bede.



Figures 28 & 29 (right): Phase diagrams for RCT data (left) and RCT and TA data plotted together (right).

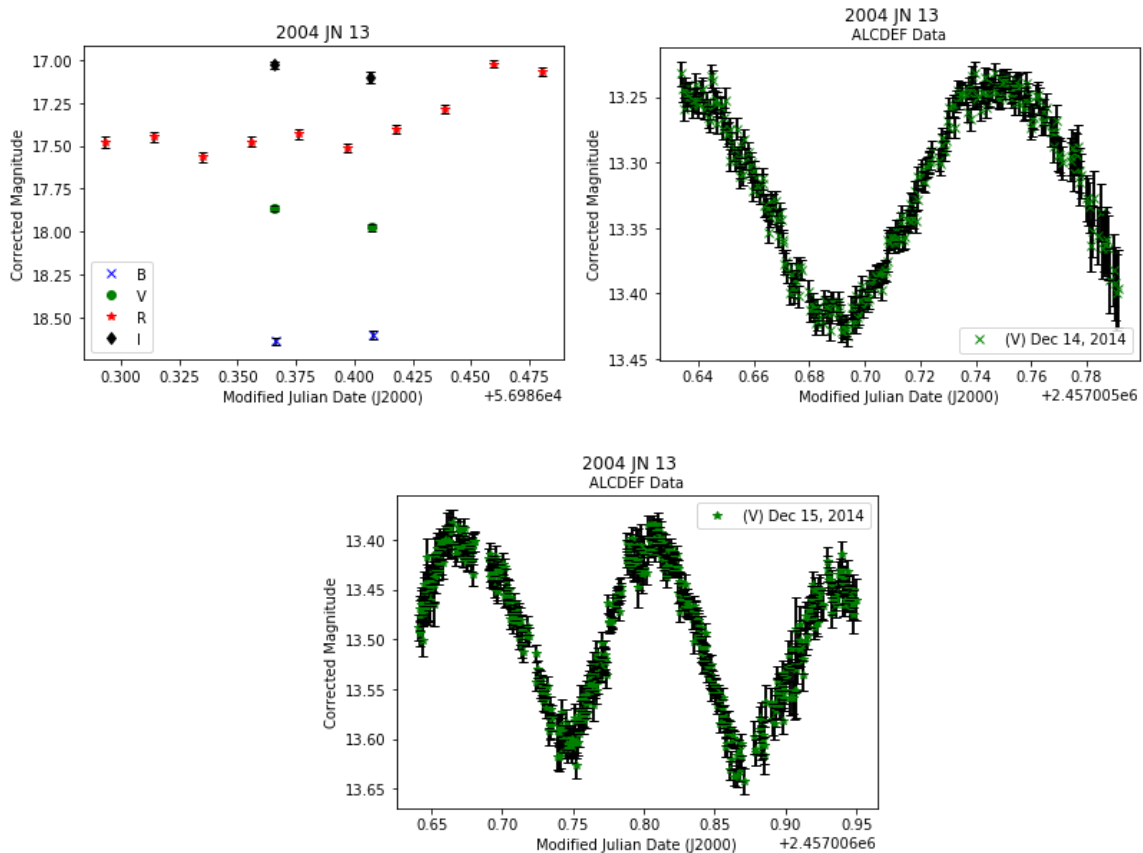


*Figures 30 & 31: Phase plots for period result 161.1501 hours showing phased TA data (left) and both data sets (TA (red) and RCT data(blue)) (right).*

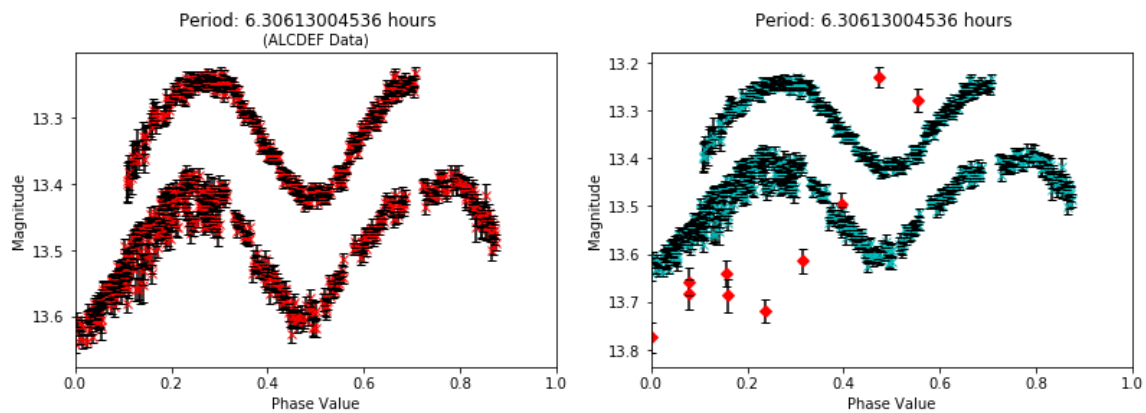
### **2004 JN 13**

Observations for asteroid 2004 JN 13 from TA consisted of B, V, R, and I images taken over a span of about 4.2 hours with the majority of observations in R band (light curve shown in Figure 32). Additional photometric data used in analysis is shown in Figures 33 and 34.

A period analysis gave a result of 6.3061 hours, confirming previously published values of 6.342 hours (Warner, 2015). Phase plots for period result 6.3061 are shown in Figures 35 and 36.



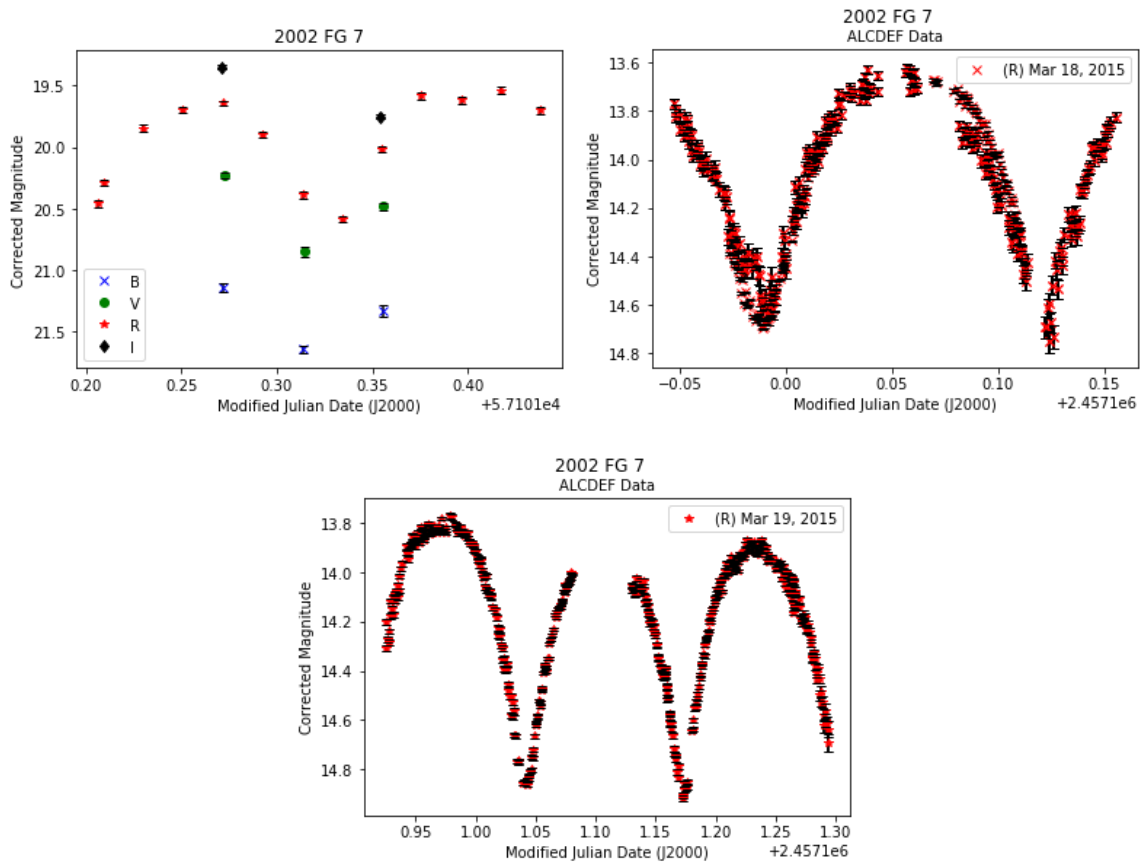
Figures 32 (upper left), 33 (upper right), & 34 (lower center): Light curves displaying TA (left) and ALCDEF data (right and lower center).



Figures 35 & 36: Phase plots for period 6.3061 hours showing ALCDEF (left) data and data from both sources (TA and ALCDEF) (right).

## 2002 FG 7

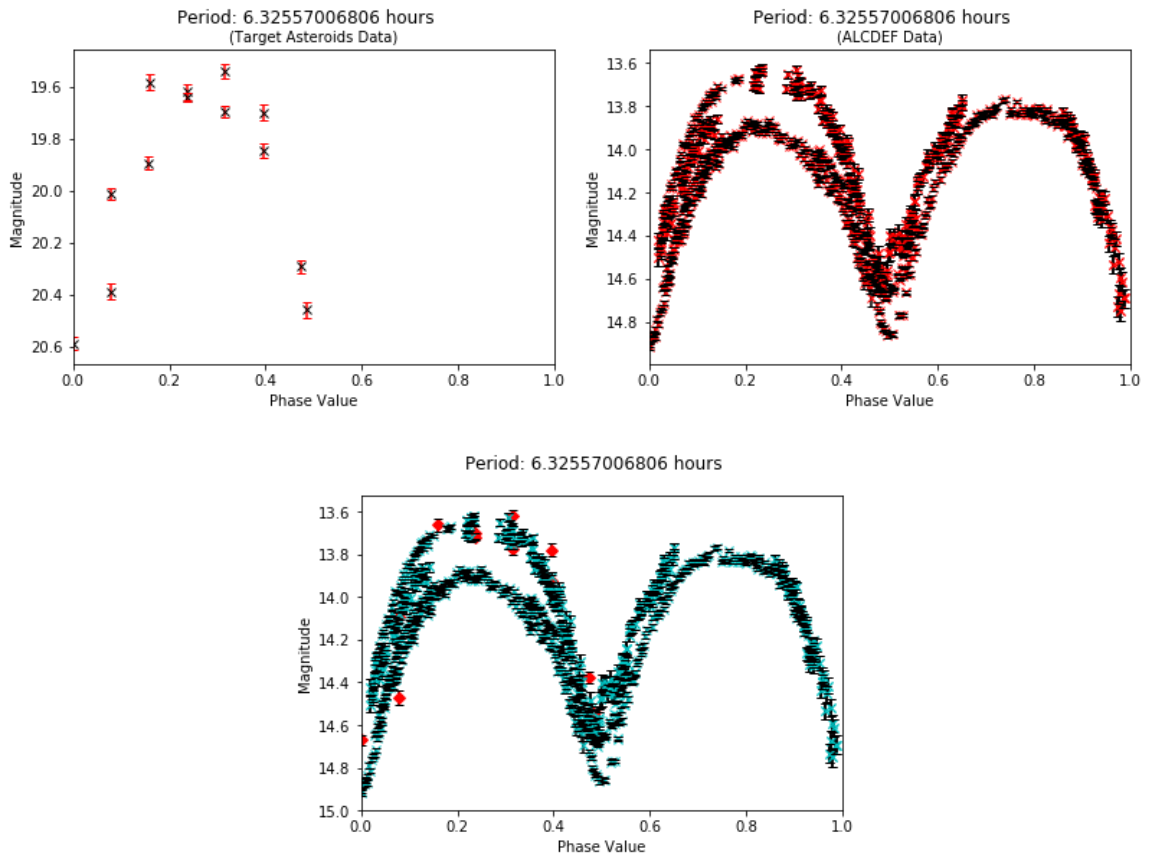
Light curves of data used for the rotational analysis of asteroid 2002 FG 7 are shown in Figures 37, 38, and 39. The Target Asteroids observations in Figure 37 consist of multi band observations acquired over a period of approximately 7 hours with the majority being in R band. 2002 FG7 is an example of an asymmetrically shaped body resulting in variation in amplitude of maxima seen in light curve, which will be discussed in greater detail in the light curve inversion section.



Figures 37 (upper left), 38 (upper right), & 39 (lower center): 2002 FG 7 light curves for TA (left) and ALCDEF data (right and lower center).

A Lomb-Scargle periodogram analysis of 2002 FG 7 yielded a period of 6.326 hours with a false alarm probability of  $9.02 \times 10^{-204}$ . This is in agreement with the

previously published value of 6.306 (Warner 2015, Oey & Groom 2017). The data set obtained from Target Asteroids was somewhat sparse, but phased well with photometric data from ALCDEF. Figures 40 and 41 show the phase plots for a period of 6.326 hours for Target Asteroids data, and ALCDEF data respectively. Figure 42 displays the phase plot for both data sets.

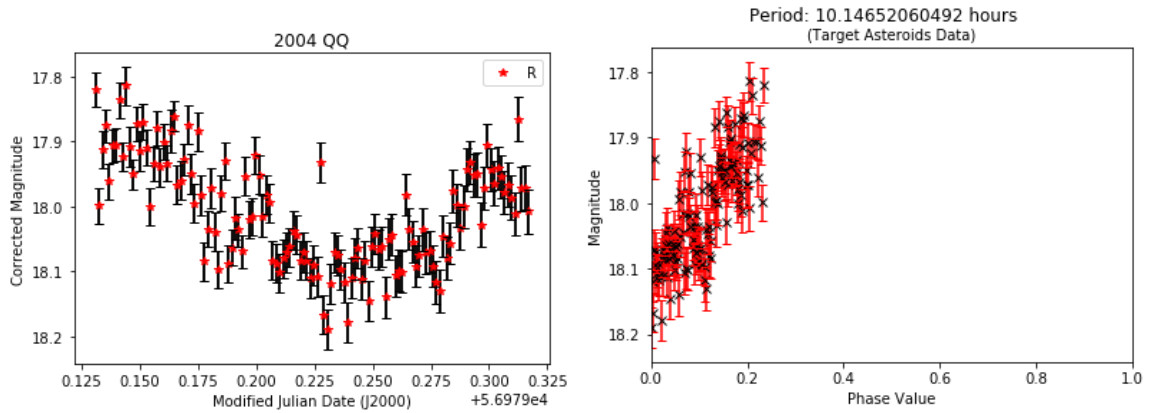


*Figures 40 (upper left), 41 (upper right), & 42 (lower center): Phase plots for period result 6.3256 hours.*

### **2004 QQ**

Asteroid 2004 QQ was a challenge as the data from TA was sparse and no ALCDEF data was available for this target. TA data consisted of continuous R band observations spanning approximately 4.8 hours, equating to about half the published rotation cycle of

8.879 hours (Warner, 2015), which is noted be uncertain by 30% due to lack of full coverage of data (JPL Small Body Database, 2018). Lomb-Scargle period analysis yielded a rotation period of 10.1465 hours, which is within the 30% uncertainty window of the cited rotation period.



Figures 43 (left) and 44 (right): Light curve of 2004 QQ from TA (left) and phase plot for period 10.1465 hours (right).

### **2004 BL 86**

Unfortunately, photometry could not be performed on TA observations of asteroid 2004 BL 86 due to inability to match fields in MPO Canopus software. This body was also unobservable by the RCT during the course of this project. However, available data from ALCDEF was used to verify accuracy of analysis methods used in this work as 2004 BL 86 is a well-studied asteroid and presents an interesting example of a binary system. Asteroid 2004 BL 86 has a smaller a companion “moon” asteroid approximately 70 meters in diameter, discovered during the asteroid’s close approach on January 26, 2015. (NASA/JPL-Caltech, 2015) The main asteroid body has a diameter of approximately 325 meters. NASA JPL estimates that 16% of asteroids may have binary companions. (NASA/JPL-Caltech) Figure 45 shows an example light curve for this system from data

taken near the time of close approach. Systems of this type show a more complex light curve as there is variability due rotation about an axis and variability due to orbit of smaller companion body around main asteroid body, thus two periods are present: rotation period and binary period. The rising amplitude of the overall light curve in Figure 45 is likely from the presence of the orbiting moon, the effects of which would be easier to discern at times when the bodies are close to earth due to increased quality of observations (i.e. increased signal to noise ratio of observations). Previous works give a rotation period of 2.6205 hours. Analysis of available ALCDEF data yielded a similar result of 2.6167 hours. The phase plot for this result is shown in Figure 46.

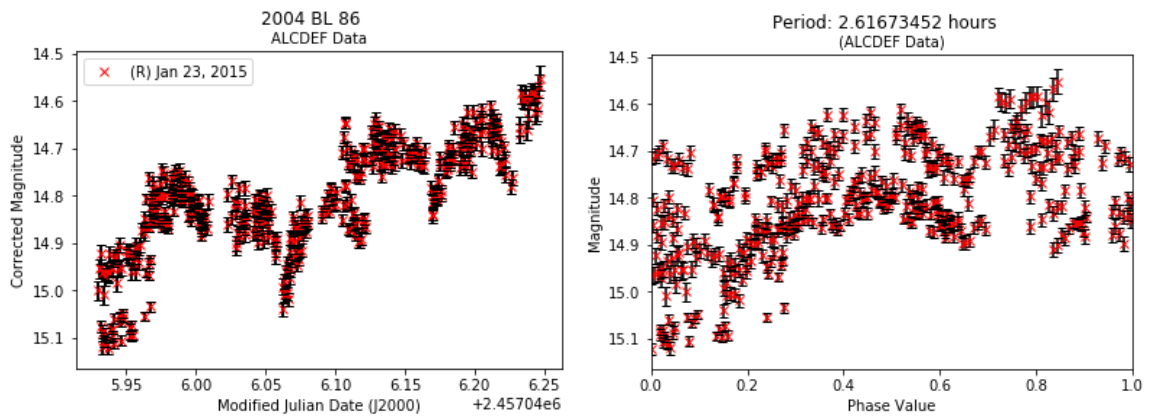


*Figure 45 & 46 (right): Example light curve of ALCDEF photometric data for 2004 BL 86 left). The phase diagram for period result 2.6167 hours (right).*





*Figure 47: Goldstone radar image of 2004BL86 from Goldstone during its close approach with earth, January 26, 2015. The companion moon can be seen at the top of the image. (Image Credit: NASA/JPL-Caltech, 2015)*

### ***Structure Modeling***

Light curve inversion requires a large set of observations covering a broad range of observing geometries (wide phase angles) to produce unique solutions. The more data available, the finer the structural detail (greater number of surface facets) the algorithm can identify, raising confidence in the uniqueness of the solution. (Santana-Ros, 2017) Sufficient data existed for the modeling of 2002 FG7, 2004 JN13, and Icarus. Table 4 summarizes data used in modeling for each target. Photometric data was divided into light curve “blocks” with each block containing observations from a single date. The phase angle range describes the span of phase angles covered in the observations and the last column gives the total number of photometric data points used in analysis.

	<b>Phase Angle Range of Data (degrees)</b>	<b>Number of Light Curve Blocks</b>	<b>Number of Data Points</b>
<b>2002 FG7</b>	51	27	1256
<b>2004 JN13</b>	50	7	772
<b>Icarus</b>	66	50	1120

*Table 4: Summary of data used in light curve inversion for each target modeled.*

### **2002 FG7**

Modeling of asteroid 2002 FG7 produced an asymmetric, somewhat egg-like shape with 994 vertices and 1,984 facets. The pole direction results gave an ecliptic polar angle ( $\beta$ ) of -30.821 degrees and longitude ( $\lambda$ ) of 252.782 degrees. The structure model is shown in Figure 48 from varying viewing angles. The red vector indicates the pole direction. The asymmetric shape was expected for this asteroid due to the uneven amplitudes of subsequent maxima seen in its light curve. The derived rotation period for this structure was found to be 6.3180 hours, in agreement with the Lomb-Scargle period result of 6.3257 hour

s

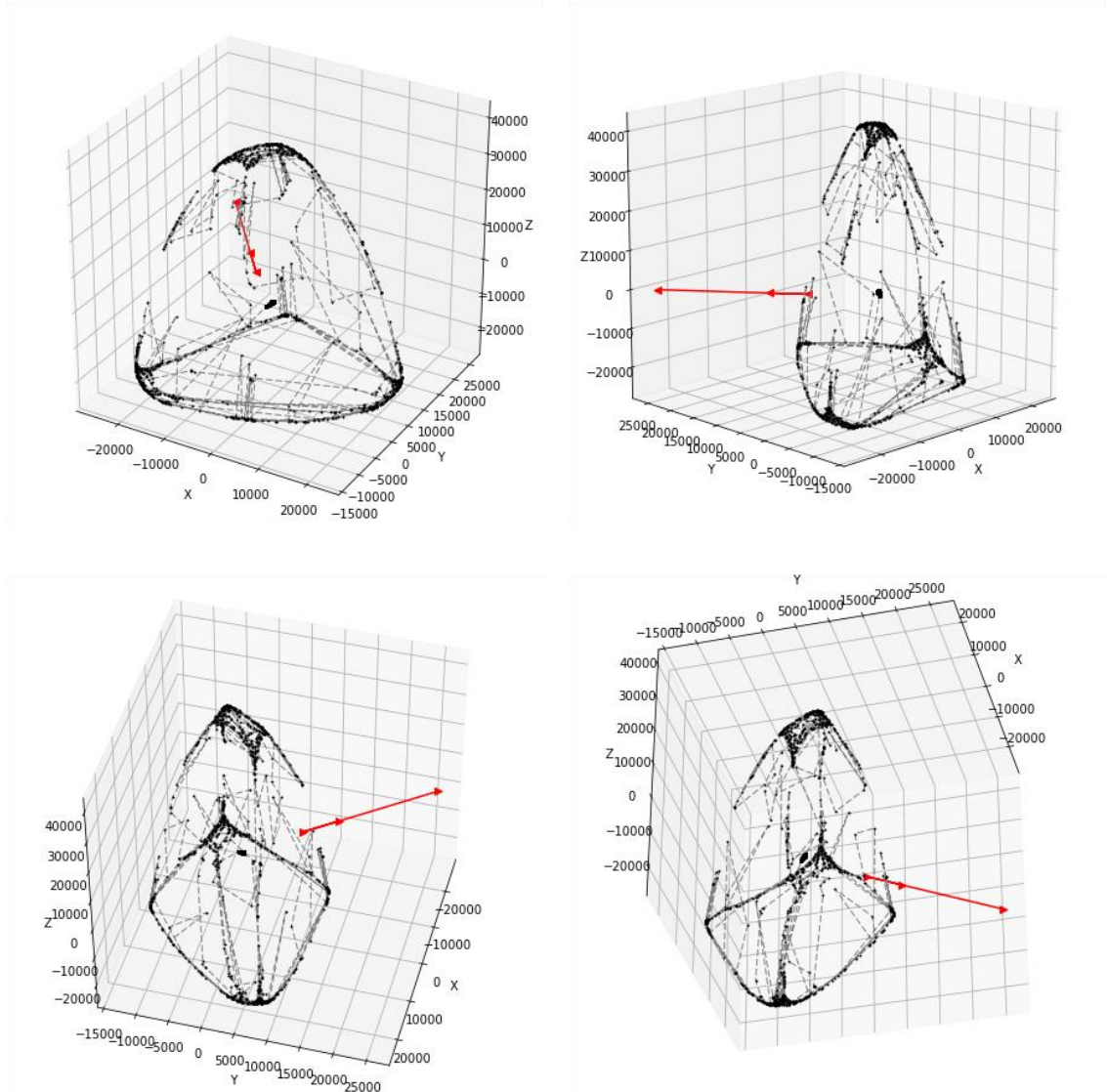


*Figure 48: Shape model for 2002 FG7 with pole direction as viewed from several angles.*  
**2004 JN13**

Shape modeling of asteroid 2004 JN13 yielded a pole solution of  $\beta = +16.307$  degrees and  $\lambda = 246.477$  degrees. The overall shape solution consisted of 1,022 vertices and 2,040 facets producing a somewhat symmetric structure as seen in Figure 49. The pole direction is indicated by the red vector. The rotation period of this structure was found to be 6.3124 hours in agreement with the 6.3061 hour period found in the Lomb-Scargle period analysis.

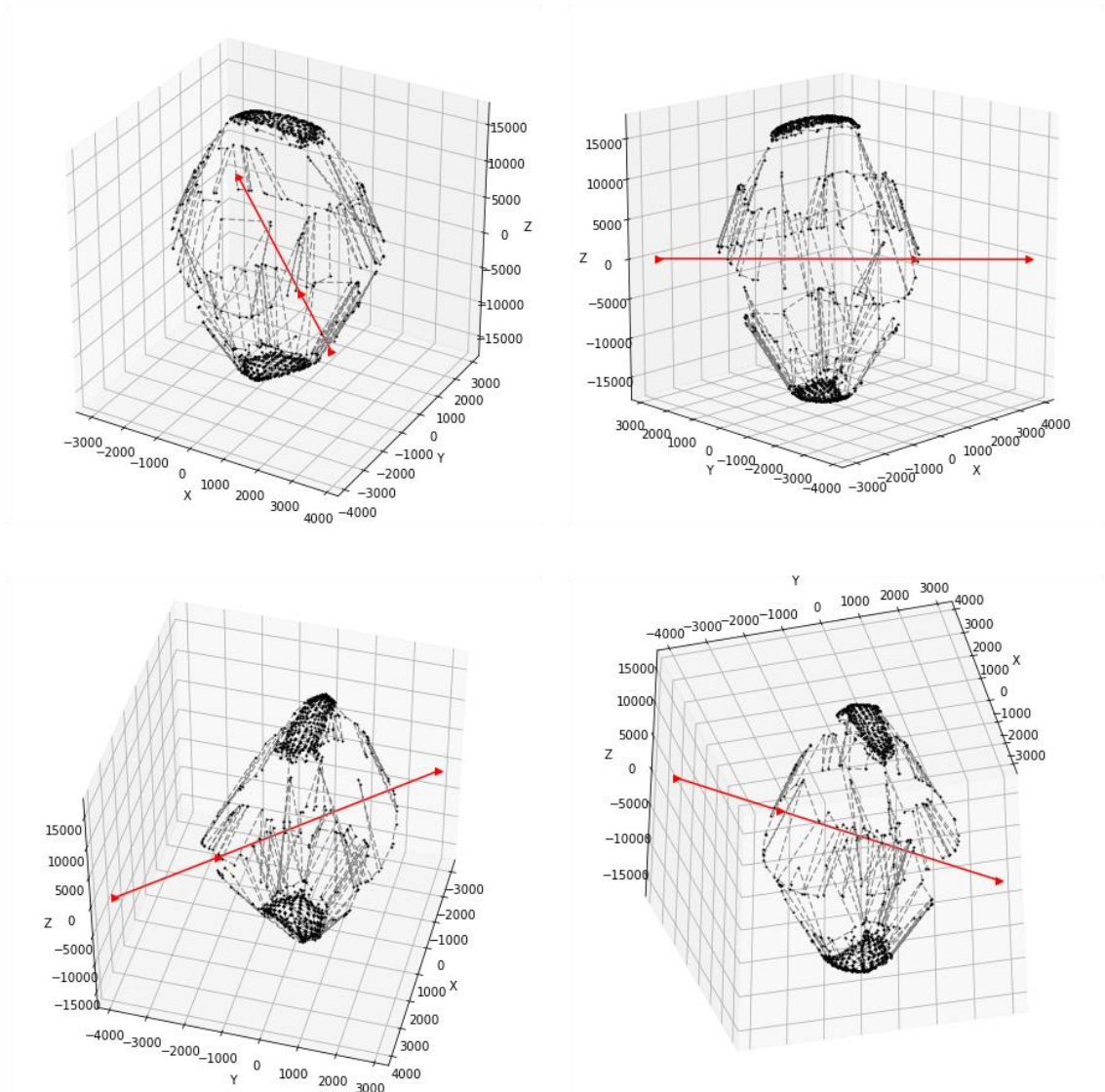


*Figure 49: Shape construction of 2004 JN13 with pole direction from various viewing angles.*

***Icarus***

The shape solution for Icarus consisted of 1,016 vertices and 2,028 facets with a pole direction of  $\lambda = 76.047$  degrees and  $\beta = +14.076$  degrees. The shape model for Icarus is displayed in Figure 50 as seen from several viewing angles. . A derived rotation period for structure in Figure 50 was computed to be 2.1577 hours, in agreement with is the result of 2.1579 hours found in the Lomb-Scargle period analysis of data.

This model yielded a more detailed structure compared to that of 2004 JN13, showing how the number of data points used in the computation affect the quality of the solution.

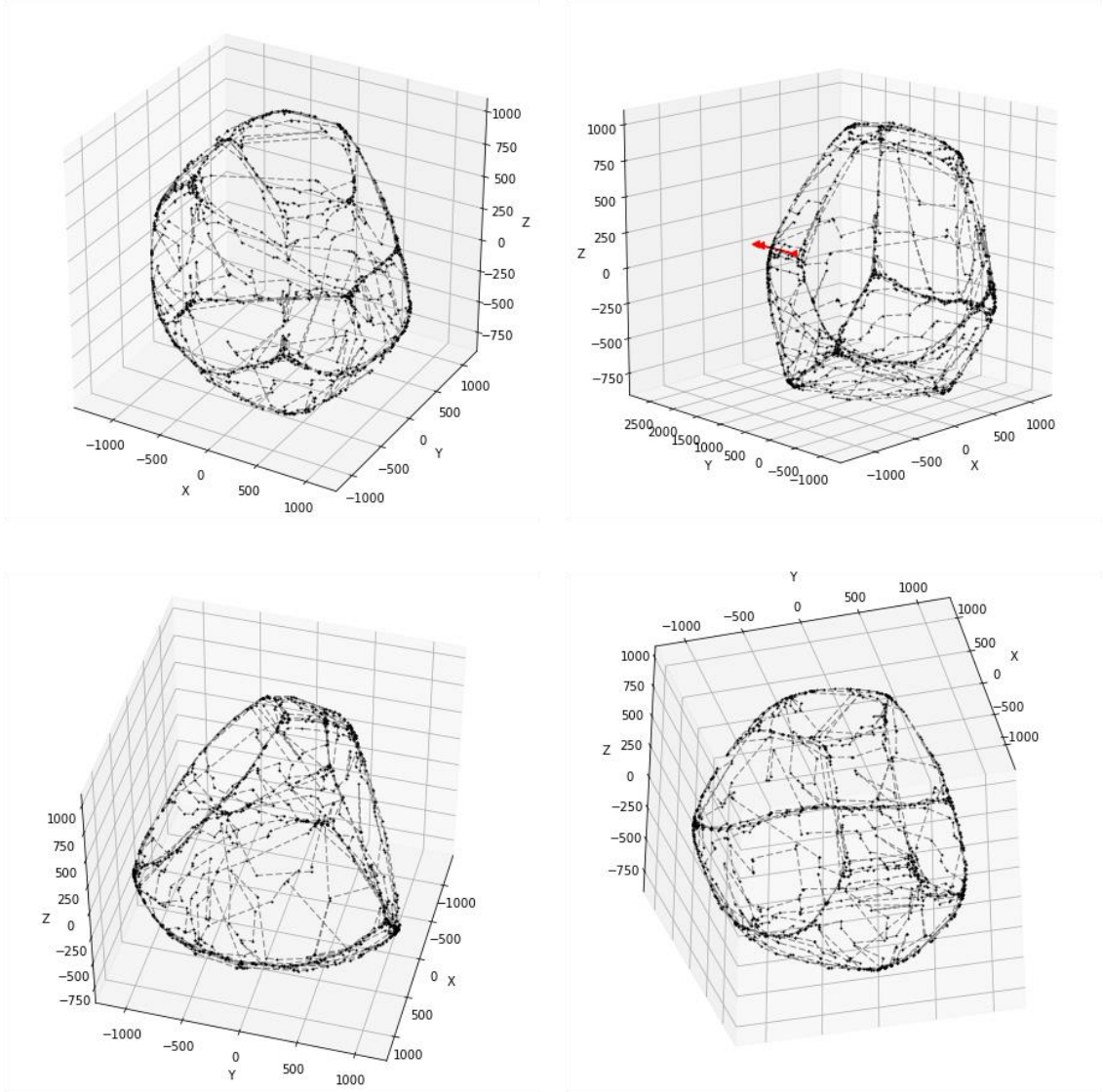


*Figure 50: Shape model for Icarus as viewed from various angles.*

## **Chapter 5**

### **Conclusions**

Observations from NASA's Target Asteroids campaign and observations obtained from the RCT (along with additional photometric data from ALCDEF) were analyzed in the characterization of rotation period and structure of eight potentially hazardous near earth asteroids. The primary results of this thesis are summarized in Tables 5 and 6. A summary of the rotation period determined for each target from the Lomb-Scargle method are given in Table 5, including comparison to period values found in other works. Additional rotation periods indicated by the analysis are listed for Bede, Hathor, and Phaethon. Further analysis using techniques appropriate for detection of multiple periodicities is needed for confirmation of these secondary period results. Table 6 gives a summary of the results of the light curve inversion modeling for 2002 FG7, 2004 JN13, and Icarus, which includes rotation axis pole direction, structural information for the modeled body, as well as rotation period values calculated for the derived structures. A search of the DAMIT (Database of Asteroid Models via Inversion Techniques) database and literature search yielded no previous light curve inversion models for 2002 FG7, 2004 JN13, or Icarus at the time of this presentation, thus, these are believed to be the first such models for these bodies.

Target	Period ( <i>this work</i> ) (hours)	False Alarm Probability	Published Period (hours)
2002 FG 7	6.3257	9.02E-204	6.306
2004 BL 86	2.6167	5.60E-25	2.6205
2004 JN 13	6.3061	1.08E-217	6.342
2004 QQ	10.1465	1.31E-26	8.879
Bede (RCT Data)	228.8961	2.31E-08	226.8
Bede (TA data)	161.1501	3.37E-143	226.8
Hathor	3.3771	5.28E-16	3.350
Hathor (Possible)	2.2169	4.98 e-46	3.350
Icarus	2.1579	9.44E-22	2.2726
Phaethon	3.6043	6.40E-62	3.604
Phaethon	4.5563	7.43E-38	3.604

Table 5: Rotation period results summary with comparison to previously published periods.

	$\lambda$ (degrees)	$\beta$ (degrees)	Vertices	Facets	Period from Inversion (hours)
<b>2002 FG7</b>	252.782	-30.821	994	1,984	6.3180
<b>2004 JN13</b>	246.477	+16.307	1,022	2,040	6.3124
<b>Icarus</b>	76.047	+14.076	1,016	2,028	2.1577

Table 6: Summary of light curve inversion modeling analysis results.

The complex and diverse nature of asteroid bodies poses unique challenges in the observation and characterization of these bodies. As evident in this work, much information can be discerned given the availability of large quantities of quality observations. Light curve inversion modeling is a relatively new technique; although based on sound methodologies, there is some uncertainty as to the precise amount of data needed for unique solutions. In addition to the number and quality of observations needed, a wide range of viewing geometries in observations is essential to the reliability of model solutions. The surface albedo of the asteroid is also assumed to be relatively constant across

the facets, which depends on the composition of the asteroid being consistent. While modeling of monolithic single body structures is better studied, many asteroids have rubble pile structures as seen with Bede, or consist of multiple bodies or binary systems as seen with 2004 BL86. Modeling of these structures requires more in-depth computational analysis which has not been rigorously studied using light curve inversion techniques.

Additional challenges arise when working with data from multiple sources. Offsets in instrumental magnitudes must be calculated, which can be difficult if the photometric data does not cover a complete rotation cycle due to variability in subsequent peak magnitudes seen in asteroid light curves. The importance of appropriate sampling of observations also becomes apparent when attempting rotation period analysis due to this challenge.

Since asteroids exhibit variability due to position in orbit and phase, magnitudes must be corrected to reduced magnitude so that any remaining variability can be assumed to be caused by rotation about an axis and structural features. The amount of computation that must be undertaken before meaningful analysis can begin is quite daunting and time consuming. However, this endeavor is worthwhile as it provides vital information about bodies that pose a potential threat of collision with earth. While detection of asteroids and orbit solutions is essential to the prediction of impact events, likewise, structural analysis of these bodies is essential to interception, deflection and mitigation in the event of a predicted impact. The technology to allow direct optical observation of many asteroids is limited, due to the size and relative dimness of most potentially hazardous asteroids. Thus, shape modeling can give a structural description we could not see otherwise, allowing for



greater knowledge of physical characteristics vital to the planning of intercept and impact mitigation strategies.

### ***Future Work***

As with any sound scientific practice, the reliability of solutions is confirmed by the ability to produce similar results in future work. Thus, shape analysis with multiple data sets producing similar solutions would provide evidence as to the viability of models. Future analysis utilizing data with greater observational coverage is needed to fine tune shape and period solutions. For targets with complex rotational behavior (tumbling), more rigorous analytic methods than those used here should be undertaken to extract the multiple periods present in the photometric data.

## References

- "Asteroid That Flew Past Has a Moon"*. (2015). Retrieved from NASA Jet Propulsion Laboratory California Institute of Technology:  
<https://www.jpl.nasa.gov/news/news.php?feature=4459>
- "Asteroids in Depth"*. (2017). Retrieved from NASA Science Solar System Exploration:  
<https://solarsystem.nasa.gov/planets/asteroids/indepth>
- "Interactive Map of Meteor Strikes"*. (2017). Retrieved from The Meteorological Society:  
<https://www.lpi.usra.edu/meteor/metbull.php>
- "Minor Planet Discoverers (by number)"*. (2017, January 12). Retrieved from Minor Planet Center.
- "Near Earth Asteroids - A Chronology of Milestones 1800-2200"*. (2013, October 7). Retrieved from International Astronomical Union:  
<https://www.iau.org/public/themes/neo/nea2>
- (2017). Retrieved from B612 Foundation: <https://b612foundation.org/>
- Ansdell, M., Meech, K., Hainaut, O., Buie, M., & al., e. (2014). *Astrophysics Journal* 793, A50.
- Barensteen, G. (2013, February 15). *"How often do large meteoroids hit us?"*. Retrieved from <http://www.geert.io/the-frequency-of-large-meteoroids.html>

Behrend, R. (2018). Retrieved from Observatoire de Geneve :

[http://obswww.unige.ch/~behrend/page\\_cou.html](http://obswww.unige.ch/~behrend/page_cou.html)

Binzel, R. (2000). "The Torino Impact Hazard Scale". *Planetary and Space Science, Vol 48*, p. 297-303.

Birlan, M., Popescu, M., Nedelcu, D., Turu, V., & al., e. (2015). *Astronomy Astrophysics 581*, A3.

Brown, P., Spalding, R., ReVelle, D., Tagliaferri, E., & Worden, S. (2002, November 12). The flux of small near Earth objects colliding with the Earth. *Nature*, p. 294-296.

Buchheim, R. (2010). Methods and Lessons Learned Determining the H-G Parameters of Asteroid Phase Curves. *The Society for Astronomical Sciences 29th Annual Symposium on Telescope Science*, p. 101-115.

Burgett, W. S., Miller, P., PS1SC, & IASC. (2011). "The First Pan-STARRS Asteroid Search Campaign: Astronomical Discovery Program for High School Students". *AAS Meeting # 218, Bulletin of the American Astronomical Society, Vol 43 ID 215.03*.

Carbognani, A. (2015). *Minor Planet Bulletin 43*, 290-295.

Chamberlin, A., Chesley, R., Chodas, W., Giorgini, D., Keesey, S., Wimberly, N., & Yeomans, D. (2001). "Sentry: An Automated Close Approach Monitoring System for Near Earth Objects". *Bulletin of the American Astronomical Society, Vol 33*, p. 1116.

- Chesley, S. R., Chodas, P. W., Milani, A., Valsecch, G. B., & Yeomans, D. K. (2002). "Quantifying the risk posed by potential Earth impacts". *Icarus*, Vol 159, p. 423-432.
- Council, S. S. (2008). "Defending Planet Earth: Near Earth Object Surveys and Mitigation Strategies". National Academy Press.
- De Angelis, G. (1995). *Planetary Space Science* 43, 649-682.
- Garber, M. (2013, February 15). "Meteorite strikes are actually quite common". *The Atlantic*. Retrieved from theatlantic.com:  
<https://www.theatlantic.com/technology/archive/2013/02/meteorite-strikes-are-actually-quite-common/273211>
- Gehrels, T., Roemer, E., Taylor, R., & Zellner, B. (1970). *Astronomy Journal* 75, 186-195.
- Goldstone Radar Observations Planning 1566 Icarus*. (2015). Retrieved from JPL Asteroid Radar Research:  
[https://echo.jpl.nasa.gov/asteroids/Icarus/Icarus\\_planning.html](https://echo.jpl.nasa.gov/asteroids/Icarus/Icarus_planning.html)
- Goldstone Radar Observations Planning: 2340 Hathor, 2014 SM143, 2014 RQ17, 2014 TV, and 2014 SC324*. (2014). Retrieved from JPL Asteroid Radar Research:  
[https://echo.jpl.nasa.gov/asteroids/Hathor/Hathor\\_planning.html](https://echo.jpl.nasa.gov/asteroids/Hathor/Hathor_planning.html)
- Hanus, J., Delbo, M., Vokrouhlicky, D., Pravec, P., & al., e. (2014). *Astronomy Astrophysics* 586, A108.

Harrington, M. (2012, January 12). *Asteroids*. Retrieved from Lowell Observatory:

<https://lowell.edu/asteroids>

Hatch, P., & Wiegart, P. A. (2015). "On the rotation and axis ratios of the smallest known near Earth asteroids-the archetypes fo the Asteroid Redirect Mission targets".

*Planetary and Space Science, Vol 111*, p. 1-168.

*IASC Campaigns*. (2017). Retrieved from International Asteroid Search Collaboration:

<http://iasc.hsutx.edu.html>

*JPL Small Body Database*. (n.d.). Retrieved from NASA.gov:

<https://ssd.jpl.nasa.gov/sbdb.cgi>

*JPL Small-Body Database Browser*. (2018). Retrieved from Jet Propulsion Laboratory:

<https://ssd.jpl.nasa.gov/sbdb.cgi>

Kaasalainen, M., & Durech, J. (2018). *DAMIT Software Downloads*. Retrieved from

Database of Asteroid Models from Inversion Techniques (DAMIT):

[http://astro.troja.mff.cuni.cz/projects/asteroids3D/web.php?page=download\\_software](http://astro.troja.mff.cuni.cz/projects/asteroids3D/web.php?page=download_software)

Kaasalainen, M., & Torppa, J. (2001). "Optimization Methods for Asteroid Lightcurve

Inversion I: Shape Determination". *Icarus, Vol 153*, p. 24-36.

Kaasalainen, M., Torppa, J., & Muinonen, K. (2001). "Optimization Methods for

Asteroid Lightcurve Inversion II: The Complete Inverse Problem". *Icarus, Vol*

*153*(Issue 1), p. 37-57.

- Kinoshita, D., Ohtsuka, K., Ito, T., Miyasaka, S., Nakamura, T., Abe, S., & Chen, W.-P. (2017). "Rotationally time resolved vis spectroscopy of 3200 Phaethon". *The Astrophysical Journal*. Retrieved from <https://arxiv.org/abs/1703.00296v1>
- Klinglesmith, D. I., Hanowell, J., & Hendrickx, S. (2015). *Minor Planet Bulletin* 42, 158-159.
- Krugly, Y., Bel'skaya, I., Shevchenko, V., & al., e. (2002). *Icarus* 158, 294-304.
- LINEAR*. (2013). Retrieved from Lincoln Laboratory MIT:  
<https://www.ll.mit.edu/mission/space/linear>
- Lomb, N. (1976). "Least-squares frequency analysis of unequally spaced data". *Astrophysics and Space Science, Vol 39*, p. 447-462.
- Mainzer, A., Bauer, J., Gray, T., Masiero, J., Cutri, R., Dailey, J., . . . et.al. (2011). "Preliminary Results from NEOWISE: An Enhancement to the Wide-Field Infrared Survey Explorer for Solar System Science". *The Astrophysical Journal*, 731(Issue 1 Article ID 53), 13.
- Marcus, R., Melosh, H. J., & Collins, G. (2010). "*Earth Impact Effects Program*". Retrieved from <https://impact.ese.ic.ac.uk/ImpactEarth/ImpactEffects/>
- Meech, K., Hainaut, O., & Buie, M. (1996). *Abstracts of ACM 1996*, 42.
- Miner, E., & Young, J. (1969). *Icarus* 10, 436-440.
- MinorPlanet.Info LCDB: Summary Table Query*. (2018). Retrieved from Light Curve Database (LCDB): <http://www.minorplanet.info/PHP/lcdbsummaryquery.php>

- Morrison, D., Chapman, C., Steel, D., & Binzel, R. (2004). "Impacts and the Public Communicating the Nature of the Impact Hazard". *Mitigation of Hazardous Comets and Asteroids*, p. 353.
- MPC Publications and Services*. (2017). Retrieved from The International Astronomical Union Minor Planet Center: <http://www.minorplanetcenter.net/iau/mpc.html>
- NEO Basics*. (2017). Retrieved from Jet Propulsion Laboratory Center for Near Earth Object Studies: [https://cneos.jpl.nasa.gov/about/neo\\_groups.html](https://cneos.jpl.nasa.gov/about/neo_groups.html)
- NeoDyS Risk List*. (2018). Retrieved from NEODyS-2 Near Earth Objects - Dynamic Site: <http://newton.dm.unipi.it/neodys/index.php?pc=4.1>
- Oey, J., Williams, H., & Groom, R. (2017). *Minor Planet Bulletin* 44, 200-204.
- OSIRIS REx Mission Details*. (2017). Retrieved from OSIRIS REx Mission Webpage: <https://www.asteroidmission.org/mission>
- Palermo Technical Impact Scale*. (2002). Retrieved from JPL Center for Near Earth Object Studies: [https://cneos.jpl.nasa.gov/sentry/palermo\\_scale.html](https://cneos.jpl.nasa.gov/sentry/palermo_scale.html)
- Pan, S.-S., Abe, S., & Kinos, D. (2012). *ACM* 2012, 6294.
- Planetary Defense Frequently Asked Questions*. (2017, August 17). Retrieved from NASA Planetary Defense: <https://www.nasa.gov/planetarydefense/faq>
- Polishook, D. (2017). "*Spin Evolution Mechanisms of Asteroids*". Retrieved from <http://wise-obs.tau.ac.il/~david/OnSpinEvolution.htm>
- Pollock, J., Pravec, P., Oey, J., & al., e. (2015). *CBET*, 4063.

- Pravec, P., & al., e. (2005). *Icarus* 173, 108-131.
- Pravec, P., Wolf, M., & Sarounova, L. (1998). *Icarus* 136, 124-153.
- Pravec, P., Wolf, M., & Sarounova, L. (2004). Retrieved from  
<http://www.asu.cas.cz/~ppravec/neo.html>
- Pravec, P., Wolf, M., & Sarounova, L. (2014). <http://www.asu.cas.cz/~ppravec/neo.html>.
- Press, W., & Rybicki, G. (1989). "Fast algorithm for spectral analysis of unevenly sampled data". *Astrophysical Journal, Part 1, Vol 338*, p. 277-280.
- Reddy, V., Gary, B., Sanchez, J., & Takir, D. e. (2015). *Astrophysics Journal* 811, A65.
- Santana-Ros, T., Duzinsky, G., & and Bartczak, P. (2017). "Shape models and physical properties of asteroids". *Assessment and Mitigation of Asteroid Impact Hazards, Astrophysics and Space Science Proceedings, Vol. 46*, p. 55.
- Scargle, J. (1982). "Studies in astronomical time series analysis II- Statistical aspects of spectral analysis of unevenly spaced data". *Astrophysical Journal, Vol 263*(Part 1), p. 835-853.
- Schmidt, R. (2018). *Minor Planet Bulletin* 45, 131.
- Target Asteroids List*. (2014). Retrieved from OSIRIS REx Mission Webpage:  
<http://www.asteroidmission.org/wp-content/uploads/2014/08/TargetAsteroidListv71406122.pdf>
- Tholen, D. (1984). "Asteroid taxonomy from cluster analysis of photometry". *PhD Thesis*(University of Arizona, Tuscon). Retrieved from  
<https://repository.arizona.edu/handle/10150/187738>



*Torino Impact Hazard Scale*. (2004). Retrieved from JPL Center for Near Earth Object Studies: [https://cneos.jpl.nasa.gov/sentry/torino\\_scale.html](https://cneos.jpl.nasa.gov/sentry/torino_scale.html)

Vaduvescu, O., Aznar Macias, A., Tudor, V., & Predatu, M. e. (2017). *Earth, Moon, and Planets 120*, 41-100.

VanderPlas, J. T. (2017). "Understanding the Lomb-Scargle Periodogram". *The Astrophysical Journal Supplement Series, Vol 236 Number 1*. Retrieved from <https://arxiv.org/abs/1703.09824>

Warner, B. (2015). *Minor Planet Bulletin 44*, 256-266.

Warner, B. (2015). *Minor Planet Bulletin 42*, 115-127.

Warner, B. (2017). *Minor Planet Bulletin 44*, 98-107.

Warner, B., & Stephens, R. (2018). *3200 Phaethon*. Retrieved from [http://www.planetarysciences.org/PHP/CS3\\_Lightcurves.php](http://www.planetarysciences.org/PHP/CS3_Lightcurves.php)

# Appendix A

## Abbreviations & Symbols

### *Abbreviations:*

- ALCDEF-Asteroid Light Curve Database (Photometric data)
- AU-Astronomical Unit
- DAMIT-Database of Asteroid Models from Inversion Techniques
- IRAS- Infrared Reflection-Absorption Spectroscopy
- JPL- Jet Propulsion Laboratory (NASA)
- LCDB- Light Curve Database
- MPC- Minor Planet Center
- MOID- Minimum Orbit Intersection Distance
- NASA- National Aeronautics and Space Administration
- NEA- Near Earth Asteroid
- NEAT-Near Earth Asteroid Tracking
- NEO- Near Earth Object
- OSIRIS-REx- Origins Spectral Interpretations Resource Identification Security Regolith Explorer
- PDCO-Nasa's Planetary Defense Coordination Office
- PHA- Potentially Hazardous Asteroid
- RCT-Robotically Controlled Telescope (Western Kentucky University)
- TA- Target Asteroids
- WKU- Western Kentucky University

### *Symbols:*

- e- eccentricity
- a- semi-major axis
- q-perihelion distance
- i- orbital inclination angle
- Q- aphelion distance

- $\beta$  – Astrocentric ecliptic polar angle
- $\lambda$  – Astrocentric longitude of pole direction